COVID-19 optimal vaccination policies: a modeling study on efficacy, natural and vaccine-induced immunity responses

Manuel Adrian Acuña-Zegarra[a], Saúl Díaz-Infante[b,*], David Baca-Carrasco[c], Daniel Olmos Liceaga[a]

[a] *Departamento de Matemáticas, Universidad de Sonora, Blvd. Luis Encinas y Rosales S/N, Hermosillo, Sonora, México, C.P. 83000.*

[b] *CONACYT-Universidad de Sonora, Departamento de Matemáticas, Blvd. Luis Encinas y Rosales S/N, Hermosillo, Sonora, México, C.P. 83000.*

[c] *Departamento de Matemáticas, Instituto Tecnológico de Sonora, 5 de Febrero 818 Sur, Colonia Centro, Ciudad Obregón, Sonora, México, C.P. 85000.*

Abstract

At the date, Europe and part of North America face the second wave of COVID-19, causing more than 1 300 000 deaths worldwide. Humanity lacks successful treatments, and a sustainable solution is an effective vaccine. Pfizer and the Russian Gamaleya Institute report that its vaccines reach more than 90 % efficacy in a recent press release. If third stage trial results favorable, pharmaceutical firms estimate big scale production of its vaccine candidates around the first 2021 quarter and the World Health organization fix as objective, vaccinate 20 % of the whole population at the final of 2021. However, since COVID-19 is new to our knowledge, vaccine efficacy and induced-immunity responses remain poorly understood. There are great expectations, but few think the first vaccines will be fully protective. Instead, they may reduce the severity of illness, reducing hospitalization and death cases.

Further, logistic supply, economic and political implications impose a set of grand challenges to develop vaccination policies. For this reason, health decision-makers require tools to evaluate hypothetical scenarios and evaluate admissible responses.

Our contribution answers questions in this direction. According to the WHO Strategic Advisory Group of Experts on Immunization Working Group on COVID-19 Vaccines, we formulate an optimal controlled model to describe vaccination policies that minimize the burden of COVID-19 quantified by the number of disability-adjusted years of life lost. Additionally, we analyze the reproductive vaccination number according to vaccination profiles depending on coverage, efficacy, horizon time, and vaccination rate. We explore scenarios regarding efficacy, coverage, vaccine-induced immunity, and natural immunity via numerical simulation. Our results suggest that response regarding vaccine-induced immunity and natural immunity would play a dominant role in the vaccination policy design. Likewise, the vaccine efficacy would influence the time of intensifying the number of doses in the vaccination policy.

Keywords: COVID-19, optimal control, vaccination policy vaccine profile, vaccine-induced immunity, natural immunity, reinfection, vaccine efficacy, WHO-SAGE, DALYs.

1. Introduction

1.1. Revised Introduction

Accepted state of the art plus problem to be resolved. After COVID-19 became a Pandemic in March 2020, the World Health Organization (WHO) organized a group of specialists dedicated to immunization against

*Corresponding author

Email addresses: adrian.acuna@unison.mx (Manuel Adrian Acuña-Zegarra), saul.diazinfante@unison.mx (Saúl Díaz-Infante), david.baca@itson.edu.mx (David Baca-Carrasco), daniel.olmos@unison.mx (Daniel Olmos Liceaga)

COVID-19: the SAGE Working Group on COVID-19 vaccines [1]. In July 2020, WHO SAGE published in [1] the document entitled "Prioritized infectious disease and economic modeling questions."

Here we attempt to answer some of the questions regarding the design of vaccination policies. Fortunately, the unprecedented efforts of many scientists have succeeded in developing vaccines to protect against COVID-19. When writing these sentences (February 2021), Mexico signed contracts that promise vaccine supply doses from Pfizer-BioNtech, AstraZeneca, CanSinoBio firms, and Gamaleya center. Besides, other vaccines probably get approval this year by the health authorities.

Although there are approved COVID-19 vaccine developments, its effective and fair administration implies enormous challenges. Health authorities will administrate more than one development. Each vaccine development requires different logistics, management, and capacitation. For example, the Pfizer-BioNtech vaccine requires a high-tech cold chain for its transportation.

The significant barrier at the moment is to produce enough doses to vaccinate more than half the worldwide population in record time. Making vaccines demand complex processes, so we expect more situations like Pfizer's and AstraZeneca's announced delays. Consequently, health authorities would review and recalibrate its vaccination policies according to dynamic information.

In mathematical epidemiology, the modeling of vaccination policies reached vast and impressive advances. Some approaches range from deterministic to stochastic, discrete or continuous, and based on ordinary or partial derivatives *[refs?]*. The new tendency also points towards statistical data analysis, optimization, and combinations of all mentioned techniques *[refs?]*. However, the previous studies provide limited insights into the particularities of SARS-CoV-2.

Authors' objectives. Despite new information emerges as the current pandemic evolves, the immunological responses of COVID-19 remains poorly understood . Essential and conclusive information about natural and vaccine-induced immunity remains under development [2–4]. The mutations of the SARS-CoV-2 would impact the vaccine efficacy–as in Africa's reported case with AstraZeneca [5]. Further, Johnson & Johnson reports in [6] that its vaccine efficacy differs across geographical regions.

Clearly, COVID-19 vaccination policies should endure complex and high uncertain issues. Thus, optimize the impact of the scarce vaccine supply is mandatory. In this line, we model and simulate hypothetical scenarios.

We aim to explore scenarios regarding a given vaccine profile and different natural immunity responses. Our main objective is the formulation of optimal schedules for vaccine administration that ensure the following:

- To cover a target population fraction in a fixed time horizon.
- To minimize COVID-19 burden quantified in DALYs.
- To preserve hospitalization occupancy below a required bound.

Introduction to the literature. According to Toner et al. [7], the last influenza vaccination program may share some similarities with COVID-19 in the USA, but the latter demands new requirements. Further, health authorities would need to revise and adapt current vaccination policies as the pandemic evolves. Consequently, vaccination policies design and calibration should consider other Non-Pharmaceutical Interventions (NPIs) in parallel.

Iboi et al. [8] model the effect of the combined NPIs strategies and vaccination and conclude that both are essential to mitigate the actual state of COVID-19 in the USA. Recently, [9] discusses this conducted strategy across groups differentiated according to mask-wearing. Makhoul et al. [10] analyze the impact of SARS-CoV-2 vaccination in age-stratified groups and vaccination strategies, according to reduction of susceptibility, infectiousness, duration of infection, and mitigation of severe cases.

Survey of pertinent literature. Early COVID-19 Kermack-McKendrick type models, as reported in [11–13], aim to forecast the number of cases, deaths, or hospital occupancy. Imperial College COVID-19 response team reports in [14] a data-driven model to estimate the time-dependent reproductive number. Other

COVID-19 models explore the impact of NPIs as lockdown and exit strategies [11, 15–20], or the effect of optimal serological tests as shielding [21].

To the best of our knowledge, the most popular way to model disease control strategies with optimal control is the so-called Lenhart's approach (see, for example [22]). Mainly, the literature report models that differ only in the compartmental model or functional cost. Although optimization problems in Engineering with mixed constraints—as boundary conditions or path restrictions—are routine, in Mathematical Epidemiology are uncommon.

The preprints [23–25] address the prioritization of the COVID-19 vaccine across five or more risk groups and optimize vaccine allocation. Their approaches face different prioritization policies according to vaccine efficacy and its availability. Buckner et al. [25] apply dynamic optimization with a time resolution of one month. Previous models based on dynamical optimization mainly focus on NPIs [26–28] and just a few address optimal vaccination schedules [29].

Authors' contribution. According to real pharmaceutical profiles, our contribution employs dynamic optimization to compute optimal vaccination policies with a time-dependent vaccination rate. We model vaccination strategies as an optimal control problem with mixed restrictions. Our setup allows us to minimize the burden of COVID-19 in years of life lost and satisfying constraints of hospitalization occupancy, vaccination coverage, and time horizon of doses administration. Such strategies are aligned to the policies of the WHO strategic advisory group of experts (SAGE) on COVID-19 vaccination [1]. We run numerical experiments to explore hypothetical scenarios conforming to four main topics: optimal schedules, vaccine efficacy, natural and vaccine-induced immunity.

Aim of the present work. Here we aim to explore hypothetical scenarios conforming to:

- optimal vaccine administration schedules modulated by time-dependent vaccination rate
- different vaccine profiles as efficacy and immunization periods
- natural and induced-vaccine immunity responses

Future implications.

Outline of structure. After this brief introduction, in Section 2, we formulate our vaccination model. Section 3 discusses a vaccine reproduction number. In Section 4, we establish our optimal control problem. Section 5 displays numerical experiments regarding optimal vaccination policies. Section 6 presents our discussions. We end with a conclusions section.

2. Formulation of mathematical model

We use an extension of the classical Kermack-McKendrick model. Our formulation considers vaccination and vital dynamics. To this end, for fixed time t, we split the total population $N(t)$, according to the following compartments: susceptible ($S(t)$), exposed ($E(t)$), symptomatic infectious ($I_S(t)$), asymptomatic infectious ($I_A(t)$), recovered ($R(t)$), dead ($D(t)$) and vaccinated ($V(t)$). Our formulation requires the following hypotheses:

(**H**-1) The vaccine is administered to all individuals exempting those with symptoms. Therefore, only individuals in the S, E, I_A and R classes are candidates for vaccination.
(**H**-2) The vaccine only has effects on the susceptible individuals. Thus, susceptible individuals become vaccinated at ψ_V rate.
(**H**-3) The vaccine only protects against COVID-19.
(**H**-4) Individuals get vaccinated only once during the epidemic.
(**H**-5) Once an inoculated individual gets vaccine-induced immunity, returns to the S class after a period of time (waning immunity period).

(**H**-6) The vaccine is imperfect. A fraction of individuals in V may become infected, with a lower probability than those in the S class.

(**H**-7) After a natural immunity period, the recovered population returns to the susceptible class.

Since we will explore disease dynamics that lasts from six months to one year, the model includes vital dynamics. We consider a constant population ($N(t) = N$). Thus, we assume that birth and natural death rates are the same and represented by μ. All births lie into the S class and all but class D experience natural death. Class D does not intervene in the transmission dynamics and counts reported deaths.

The infection dynamics are as follows: Susceptible individuals (S) become infected, but not infectious, when in contact with infectious individuals I_S and I_A. Exposed individuals (E) remain in their class until they become infectious and move to either I_S or I_A. Individuals in class I_S either die by disease complications or recover, whereas individuals in class I_A move to the R class after a some time. Finally, as the vaccine is considered imperfect, individuals in V move to the E class by interacting with infectious individuals I_S and I_A at a lower rate than S individuals. Figure 1 shows the compartmental model diagram which summarizes hypotheses mentioned above.

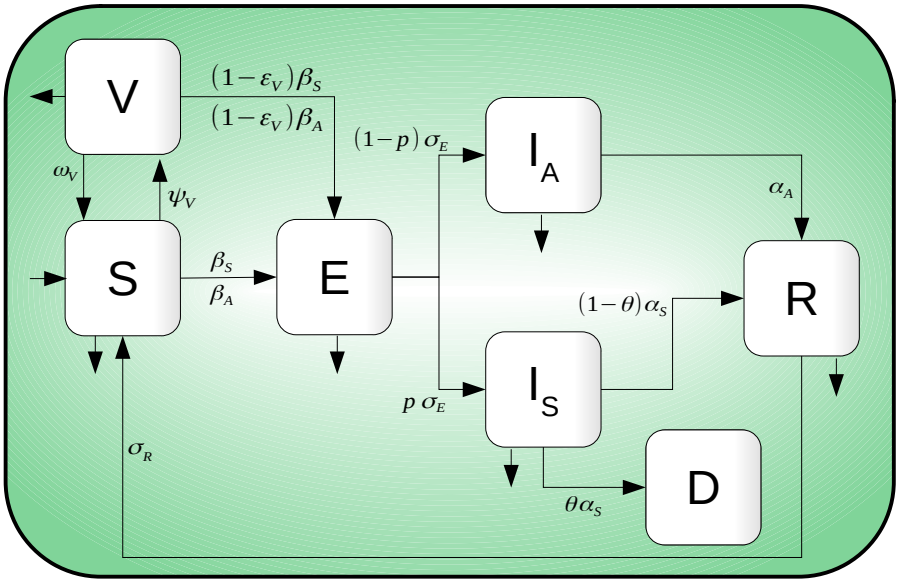

Figure 1: Compartmental diagram of COVID-19 transmission dynamics which including vaccination dynamics. Here, there are seven different classes: Susceptible (S), exposed (E), symptomatic infected (I_S), asymptomatic infected (I_A), recovered (R), death (D) and vaccinated (V) individuals.

The model is given by the following ordinary differential equations system

$$\begin{aligned}
S'(t) &= \mu\widehat{N} - f_\lambda S - (\mu + \psi_V)S + \omega_V V + \sigma_R R \\
E'(t) &= f_\lambda\,(S + (1-\varepsilon_V)V) - (\mu + \sigma_E)E \\
I_S'(t) &= p\sigma_E E - (\mu + \alpha_S)I_S \\
I_A'(t) &= (1-p)\sigma_E E - (\mu + \alpha_A)I_A \\
R'(t) &= (1-\theta)\alpha_S I_S + \alpha_A I_A - (\mu + \sigma_R)R \\
D'(t) &= \theta\alpha_S I_S \\
V'(t) &= \psi_V S - (1-\varepsilon_V) f_\lambda V - (\mu + \omega_V)V
\end{aligned} \tag{1}$$

where the infection force is defined by

$$f_\lambda := \frac{\beta_S I_S + \beta_A I_A}{\widehat{N}}. \tag{2}$$

Here, $\widehat{N}(t) = S(t) + E(t) + I_S(t) + I_A(t) + R(t) + V(t)$. For system in Equation (1) all the variables are taken normalized by the constant total population N. Therefore $\widehat{N} + D = 1$.

Let

$$\Omega = \{(S, E, I_S, I_A, R, D, V) \in [0,1]^7 : S + E + I_S + I_A + R + D + V = 1\} \subset [0,1]^7.$$

The dynamics in Equation (1) is positively-invariant on Ω (see Appendix B). Additionally, the equations

$$\begin{aligned} X'(t) &= \psi_V(S + E + I_A + R) \\ Y'_{I_S}(t) &= p\sigma_E E, \end{aligned} \tag{3}$$

count the cumulative administered vaccines doses until time t as the product $N \times X(t)$. Also, the cumulative incidence of reported cases is given by $N \times Y_{I_S}(t)$.

Remark 1. Vaccine is administered to individuals in classes S, E, I_A and R. The amount of given vaccines is quantified by Equation (3). However, as we assume the vaccine has preventive nature only, there is no change from classes E, I_A, and R to V due to vaccination.

The parameters of model Equation (1) are described in Table 1.

Parameter	Description
μ	Natural death rate
β_S (β_A)	Symptomatic (Asymptomatic) transmission contact rate
ψ_V	Vaccination rate
ω_V	Waning rate of vaccine. $1/\omega_V$ is the average time to lose vaccine-induced immunity
ε_V	Vaccine efficacy
σ_E	Latency rate. $1/\sigma_E$ is the average latency period
p	Exposed individuals' fraction who become symptomatic infectious
α_S	Transition rate from symptomatic to recover or death. $1/\alpha_S$ is the average output time of symptomatic individuals class
θ	Proportion of symptomatic individuals who die due to the disease
α_A	Recovery rate of asymptomatic individuals. $1/\alpha_A$ is the average time which asymptomatic individuals leave being infectious
σ_R	Rate of loss of natural immunity. $1/\sigma_R$ is the natural immunity period

Table 1: Parameters definition of system in Equation (1).

2.1. Calibration of baseline parameters and initial conditions

Multiple COVID-19 studies have shown important differences in transmission contact rates values across countries. For this reason, we establish a set of baseline parameter values for our geographic region of interest: the area constituted by Mexico-City and Mexico-State.

Mexico's COVID-19 database provides detailed information on reported cases, hospitalized, ambulatory and deaths. Following the ideas of *[Fergunson]*, we consider COVID-19 confirmed deaths data to calibrate both transmission contact rates and exposed individuals proportion who become symptomatic infectious.

To address this problem, we employ a MCMC method. As observation model, we use a negative binomial distribution with mean given by

$$\widehat{D}(k) = D(k) - D(k-1) = \int_{k-1}^{k} \theta\alpha_S I_S(t)dt, \tag{4}$$

where $\widehat{D}(k)$ represents the daily deaths incidence at the $k-th$ day, and $D(k)$ is the solution of the sixth equation of the system in Equation (1) without vaccination dynamics at the $k-th$ day. Figure 3 shows fitting curves with their respective confidence bands. Estimation process considers data from February 19, 2020, to October 31, 2020. Like other studies [15, 16], it is considered perturbations on both transmission contact rates due to implementing or breaking mitigation measures. For more information about the parameter estimation process, see Appendix A. Table A.9 summarizes our parameter calibration.

Parameter	Estimated range	Calibrated
β_S	[0.058 262, 0.544 492]	0.363282
β_A	[0.101 754, 0.441 215]	0.251521
p	[0.111 348, 0.249 985]	0.1213

Table 2: Estimated range for some parameters of system in Equation (1) without vaccination dynamics.

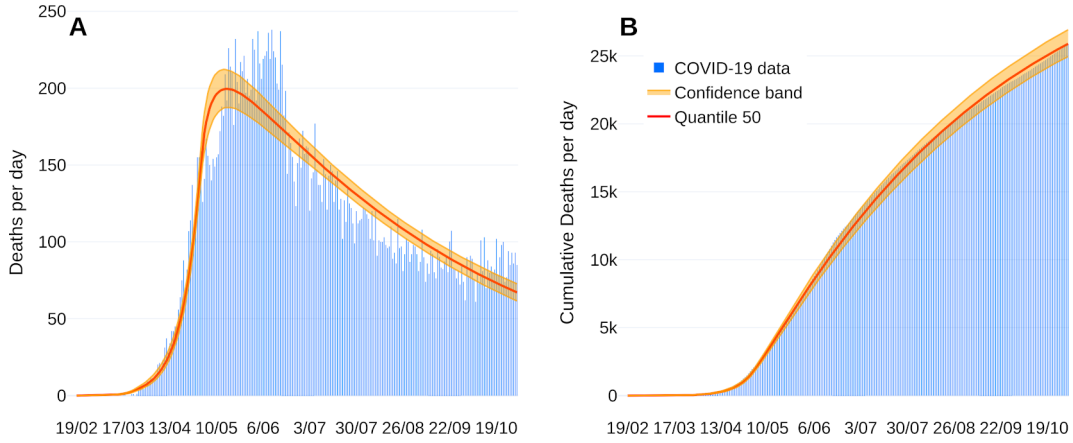

Figure 2: *Fitting death curve of the COVID-19 outbreak in Mexico-City and Mexico-State.* Panel A shows new reported deaths per day. Panel B represents cumulative deaths per day. Reported deaths data are shown in blue bars from February 19, 2020, to October 31, 2020.

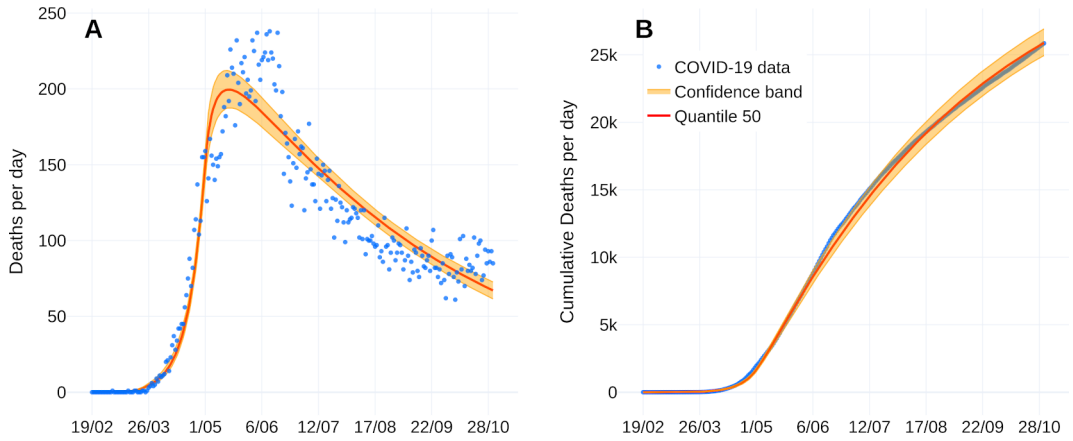

Figure 3: *Fitting death curve of the COVID-19 outbreak in Mexico-City and Mexico-State.* Panel A shows new reported deaths per day. Panel B represents cumulative deaths per day. Reported deaths data are shown in blue dots from February 19, 2020, to October 31, 2020.

3. Vaccine Reproduction Number

In this section, we present a formulation for the vaccine reproduction number. Initially, we calculate the basic reproductive number according to Van den Driessche and Watmough [30]. Then, we construct the vaccine reproduction number R_V *based on an extension of* R_0 *and show the importance of vaccination in the disease levels reduction. Our formulation will allow to formulate the disease control strategy.*

Thus, when considering *dynamics without vaccination* , the basic reproductive number is given by:

$$R_0 = \frac{p\sigma_E\beta_S}{(\mu+\sigma_E)(\mu+\alpha_S)} + \frac{(1-p)\sigma_E\beta_A}{(\mu+\sigma_E)(\mu+\alpha_A)}. \tag{5}$$

Note that each term of R_0 represents the contribution of the symptomatic and asymptomatic infectious, respectively, to the spread of the disease.

On the other hand, the vaccine reproduction number is calculated when considering vaccination dynamics given by Equation (1). Step by step calculations in Appendix B give

$$R_V = R_S + R_A, \tag{6}$$

where,

$$R_S = \frac{p\beta_S\sigma_E(\mu+\omega_V+(1-\varepsilon_V)\psi_V)}{(\mu+\sigma_E)(\mu+\omega_V+\psi_V)(\mu+\alpha_S)}, \qquad \text{and} \qquad R_A = \frac{(1-p)\beta_A\sigma_E(\mu+\omega_V+(1-\varepsilon_V)\psi_V)}{(\mu+\sigma_E)(\mu+\omega_V+\psi_V)(\mu+\alpha_A)}.$$

Following ideas of Alexander et. al. [31], expression for R_V can be rewritten as

$$R_V = R_0\,(1-f_V)\,, \tag{7}$$

where,

$$f_V = \frac{\varepsilon_V\psi_V}{(\mu+\omega_V+\psi_V)}.$$

Note that $(1-f_V) < 1$. This factor encloses parameters corresponding to the vaccine process: vaccine efficacy and waning rate (vaccine profile), and vaccination rate. Observe that if $R_0 < 1$, then $R_V < 1$. Otherwise, if $R_0 > 1$ and the following conditions hold

$$\begin{aligned} \psi_V &> \frac{(R_0-1)(\mu+\omega_V)}{(\varepsilon_V-1)R_0+1}, \\ \varepsilon_V &> 1-\frac{1}{R_0}, \end{aligned} \tag{8}$$

then R_V value is lower than one. *That is, there is a region in the parameter space in which it is possible to reduce the value of R_V below one, considering adequate efficacy, vaccination rate and duration of the effect of the vaccine. However, if the inequality (8) is not satisfied, it will not be possible to reduce the value of R_V below 1.*

To illustrate the aforementioned, Figure 4 shows the regions where it is possible to reduce the value of R_V. In this case, we set all the system parameters as given in Table 3 and fixed $\omega_V = 1/180$, leaving ε_V and ψ_V free.

Parameter	Value	References/Sources
β_S	0.363 282	Fitted
β_A	0.251 521	Fitted
α_S	0.092 506 9	[15]
α_A	0.167 504	[15]
σ_E	0.196 078	[32]
σ_R	0.002 739 73	Assumed
μ	0.000 039 138 9	Assumed
θ	0.11	Assumed
p	0.1213	Fitted

Table 3: Fixed parameters values of system in Equation (1). The parameters corresponding to vaccination are established in each scenario studied. See Table A.9 and Appendix A for more details.

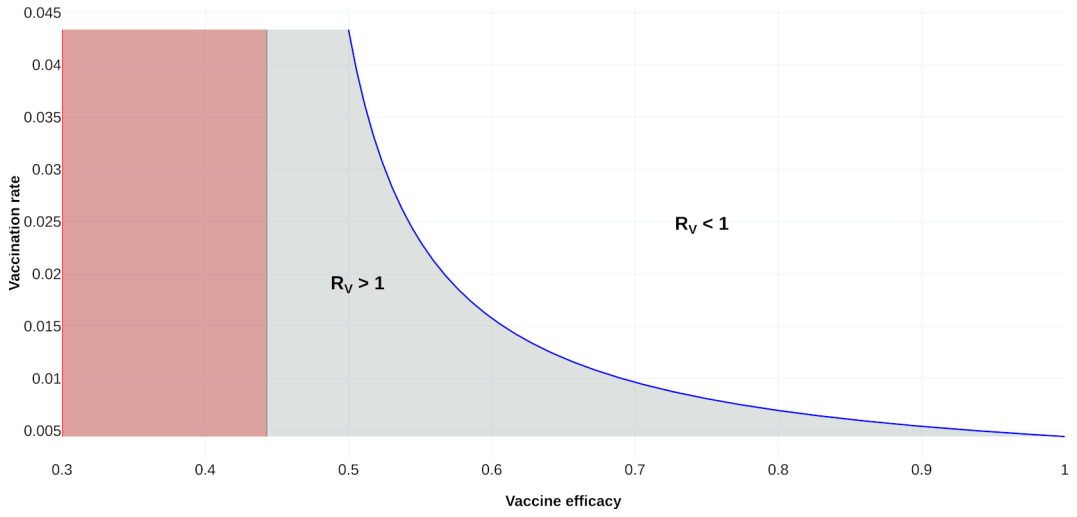

Figure 4: Plot of R_V as a function of vaccine efficacy (ε_V) and vaccination rate (ψ_V). In the gray shaded region, $R_V > 1$; and in the white region, $R_V < 1$. Note that, for our scenario, with a 50 percent vaccine efficacy and an adequate vaccination rate, it is possible to reduce the R_V value below one. The orange region is unfeasible. ~~Vaccine efficacy versus vaccination rate feasibility. In the gray shaded region $R_V > 1$ and in the white region $R_V < 1$. Note that, for our scenario, with a 50 percent vaccine efficacy and an adequate vaccination rate, it is possible to reduce the R_V value below one. The orange region is unfeasible.~~[DBC]

3.1. Baseline vaccination rate

Vaccination policies to reach a given coverage of a certain percentage of the population in a given period is of great importance. In this sense, we refer to this vaccination constant rate as the base vaccination rate, denoted by ψ_{Vbase}.

Let $W(t)$ be the normalized unvaccinated population at time t. If no individual has been vaccinated at $t = 0$, then $W(0) = 1$. Assuming that we vaccinate individuals at a constant rate ψ_{Vbase}, proportional to the actual population, we have that $W(t)$ satisfies the equation

$$\dot{W}(t) = -\psi_{Vbase} W(t) \qquad \text{with} \qquad W(0) = 1,$$

that is $W(t) = e^{-\psi_{Vbase} t}$. It implies that the number of vaccinated individuals ($\widehat{W}(t)$) at time t is given by $\widehat{W}(t) = 1 - e^{-\psi_{Vbase} t}$. Therefore, to vaccinate a fraction z of a population in the given time horizon T, it follows that ψ_{Vbase} satisfies the equation

$$z = 1 - \exp(-\psi_{Vbase}\, T)$$

thus

$$\psi_{Vbase} = \frac{-\ln(1-z)}{T}. \tag{9}$$

Observe that in the calculation of ψ_{Vbase}, it is considered all the population to be vaccinated. For our study, vaccination is not applied to symptomatic infectious individuals. Therefore, Equation (9) represents an approximation of our vaccination coverage ($x_{coverage}$) at constant rate.

Figure 5 shows the contour curves for R_V as a function of the vaccine efficacy (ε_V) and vaccination rate (ψ_V). The green line corresponds to vaccination rate ψ_{Vbase} equal to 0.000 611. With this vaccination rate, it is not possible to reduce the value of R_V below one. The intersection of the red lines correspond a vaccine efficacy equals to 0.8 and the corresponding vaccination rate such that $R_V = 1$. Note that this vaccination rate values below 0.007 implies R_V greater than 1. Thus, vaccination rate has to be greater than 0.007 in order drives R_V lower to 1. Further, a vaccine efficacy of 50 % or more is required so that, with an adequate vaccination rate, the R_V value can be reduced below one.

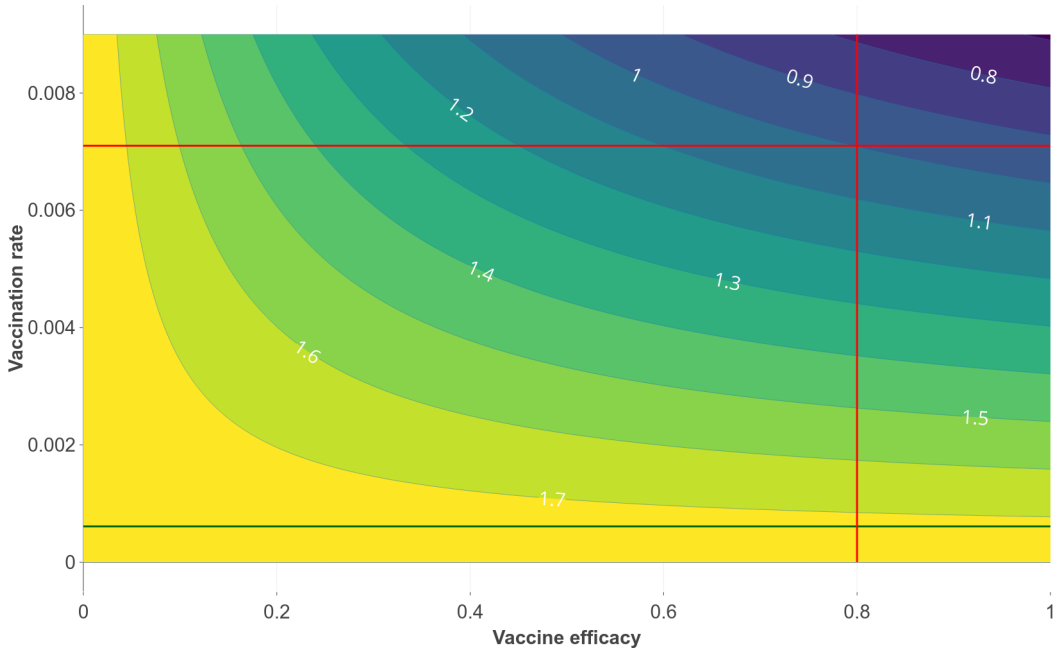

Figure 5: Contour plot of R_V, as a function of vaccine efficacy (ε_V) and vaccination rate (ψ_V) for the case where the average vaccine-induced immunity period is six month. Dark green line represents the value of $\psi_{Vbase} = 0.000\,611$, corresponding to a coverage $x_{coverage} = 0.2$ and a time horizon $T = 365$ days. Red lines show a scenario in which it is possible to reduce the R_V value below one, considering a vaccine efficacy of 0.8 and a vaccination rate of 0.007.

In the next section, the optimal control theory will be applied to propose optimal vaccination policies that minimize the COVID-19 burden.

4. Optimal Vaccination policies

In the remains of this manuscript, we use the following definitions.

Definition 1 (Constant vaccination policy). Consider the model in Equations (1) and (3). A constant vaccination policy (CP) is a policy where the vaccination rate ψ_V remains constant for all time $t \in [0, T]$. Thus the number of administered vaccine doses at time t with this CP results

$$\psi_V \left(S(t) + E(t) + I_A(t) + R(t)\right) N. \tag{10}$$

Our main idea is taking ψ_V as Equation (9) and modulating it additively by a time function $u_V(t)$. We impose that $u_V(t) \in [-m_1\psi_V, m_2\psi_V], \forall t \in [0, T]$, $m_1 \in [0, 1]$, $m_2 \in \mathbb{Q}^+$, then term

$$\psi_V + u_V(t), \tag{11}$$

amplifies or attenuates the constant vaccination rate ψ_V. If $m_1 \in (0, 1]$, then control signal $u_V(t)$ attenuates the vaccination rate ψ_V. Meanwhile, if $m_2 > 0$, then control signal $u_V(t)$ amplifies this vaccination rate.

We modify components equations corresponding to S, V, X in Equations (1) and (3) by

$$\begin{aligned} S'(t) =& \mu\widehat{N} - f_\lambda S - (\mu + (\psi_V + u_V(t))\, S \\ &+ \omega_V V + \sigma_R R \\ V'(t) =& (\psi_V + u_V(t))\, S - (1 - \varepsilon_V) f_\lambda V \\ &- (\mu + \omega_V) V \\ X'(t) =& (\psi_V + u_V(t))\, (S + E + I_A + R). \end{aligned} \tag{12}$$

Then our controlled dynamics reads

$$\begin{aligned} S'(t) &= \mu\widehat{N} - f_\lambda S - (\mu + \psi_V + u_V(t))S + \omega_V V + \sigma_R R \\ E'(t) &= f_\lambda(S + (1 - \varepsilon_V)V) - (\mu + \sigma_E)E \\ I_S'(t) &= p\sigma_E E - (\mu + \alpha_S) I_S \\ I_A'(t) &= (1 - p)\sigma_E E - (\mu + \alpha_A) I_A \\ R'(t) &= (1 - \theta)\alpha_S I_S + \alpha_A I_A - (\mu + \sigma_R) R \\ D'(t) &= \theta\alpha_S I_S \\ V'(t) &= (\psi_V + u_V(t))S - ((1 - \varepsilon_V) f_\lambda V + \mu + \omega_V)\, V \\ X'(t) &= (\psi_V + u_V(t))(S + E + I_A + R) \\ Y_{I_S}'(t) &= p\sigma_E E, \end{aligned} \tag{13}$$

$$\begin{aligned} S(0) &= S_0,\ E(0) = E_0,\ I_S(0) = I_{S_0}, \\ I_A(0) &= I_{A_0},\ R(0) = R_0,\ D(0) = D_0, \\ V(0) &= 0,\ X(0) = 0,\ Y_S(0) = Y_{S_0} \\ \widehat{N}(t) &= S + E + I_S + I_A + R + V. \end{aligned}$$

Formally we define a controlled vaccination policy as follows.

Definition 2 (Controlled vaccination policy). Conforming the model in Equation (13) we say that

$$\psi_V + u_V(t), \quad t \in [0, T],$$

is a controlled vaccination policy (CVP). Then,

$$(\psi_V + u_V(t))\, (S(t) + E(t) + I_A(t) + R(t))\, N,$$

denote the number of doses at time t according to the modulated vaccination rate $(\psi_V + u_V(t))$.

We aim to obtain time-control functions $u_V(\cdot)$ that hold natural modeling constraints—as a fixed bound for hospitalized prevalence and coverage at the final time—and optimize a conveniently cost functional. To this end, we have to assure our optimal controlled model solution, so we consider the functional space

$$\begin{aligned}\mathcal{U}[0,T] := \{&u_V : [0,T] \to \mathbb{R}, \\ &\text{such that } u_V(\cdot) \text{ bounded and} \\ &\text{piecewise continuous}\}\,.\end{aligned} \tag{14}$$

Let $x(t) := (S, E, I_S, I_A, R, D, V, X, Y_{I_S})^\top(t)$ and control signal $u_V(\cdot) \in \mathcal{U}[0,T]$. Following the guidelines of WHO-SAGE modeling questions [1], we quantify the burden of COVID-19, according to the Disability-Adjusted Life Year (DALY) indicator. Adapting DALY's definition reported in [33], we optimize the number of years of life lost with a controlled vaccination policy. Our formulation calculates a minimum of the penalization functional

$$J(u_V) = a_D(D(T) - D(0)) + a_S(Y_{I_S}(T) - Y_{I_S}(0)). \tag{15}$$

Here, a_S and a_D are parameters related to the definition of the Years of Life Lost (YLL) due to premature mortality and the Years Lost due to Disability (YLD). We estimate a_D as the average remaining life expectancy at the age of death, and according to the union of Mexico-City and Mexico-State data, we set $a_D = 7.5$ years. Parameter a_S is the product of a disability weight (DW) and the average duration of cases until remission or death in years, that is, $a_S = DW \times \alpha_S^{-1}$. Here we postulate the disability weight as the arithmetic average of disability weight regarding comorbidities reported in [34]. Our simulations employ $a_S = 0.008\,418\,473$ years. Thus, functional J penalizes the pandemic burden—in Years of Life Lost—due to mortality or disability.

To describe vaccination coverage, we ask the terminal conditon

$$\begin{aligned}\varphi(x(T)) &= X(T), \\ S(T) + E(T) + I_S(T) + I_A(T) + R(T) + V(T) + D(T) &= 1, \\ X(T) &= x_{coverage}, \\ x_{coverage} &\in \{\text{Low}(0.2), \text{Mid}(0.5)\}\,.\end{aligned} \tag{16}$$

That is, given the time horizon T, we set the vaccination coverage to 20 % or 50 % of the total population, and the rest of final states free. Likewise, we impose the path constraint

$$\Phi(x,t) := \kappa I_S(t) \le B, \qquad \forall t \in [0,T], \tag{17}$$

to ensure that critical symptomatic cases will not overload healthcare services. Here κ denotes hospitalization rate, and B is the load capacity of the health system.

Definition 3 (Admissible control vaccination policy). Let $(x(\cdot), u_V(\cdot))$ be a pair satisfying the ODE (13). Consider $\mathcal{U}[0,T]$ as in (14). If

(**AC**-1) $u_V(\cdot) \in \mathcal{U}[0,T]$
(**AC**-2) $u(t) \in [-m_1\psi_V, m_2\lambda_V]$, $\forall t \in [0,T]$, $m_i \in \mathbb{Q}$
(**AC**-3) $x(T) = (\cdot,\cdot,\cdot,\cdot,\cdot,\cdot,\cdot,x_{coverage},\cdot)^\top$
(**AC**-4) $\kappa I_S(t) \le B$, $\forall t \in [0,T]$

holds, then the CVP $\psi_V + u_V(\cdot)$ is admissible.

In other words, an admissible vaccination policy (AVP) is a CVP that satisfies the coverage and hospitalization constraints imposed on model (13). Furhter, if an AVP optimizes functional cost (15), then this AVP is an optimal vaccination policy (OVP). Formally we have the following definition.

Definition 4 (Optimal Vaccination Policy). Let $(x(\cdot), u_V(\cdot))$ a pair that satisfies the ODE (13) such that (**AC**-1)–(**AC**-4) of Definition 3 holds. Let cost functional J as in (15). If

$$\begin{aligned} J(u_V) &= \min_{u \in \mathcal{U}^\star} J(u), \\ \mathcal{U}^\star &:= \mathcal{U}[0,T] \cap \{u(\cdot) : \text{(ADC-1)–(ADC–4) holds}\}, \end{aligned} \tag{18}$$

then $\psi_V + u_V(\cdot)$ is an optimal vaccination policy.

Remark 2. Optimal vaccination amplifies or attenuates the estimated baseline ψ_V in an interval $[\psi_V^{\min}, \psi_V^{\max}]$ to optimize functional $J(\cdot)$—minimizing symptomatic incidence and death reported cases in DALYs and satisfying hospitalization occupancy and coverage constraints.

We aim to minimize the cost functional (15)—over an appropriated space—subject to the dynamics in Equation (13), coverage related to the boundary condition (16), and path constraints (17). We call this kind of policies as optimal vaccination policies (OVP). That is, we seek vaccination policies that solve the following problem.

Optimal Control Problem (OCP): Find the optimal vaccination rate $(\psi_V + u_V^*)$ such that,

$$\begin{aligned} J(u_V^*) &= \min_{u_V \in \mathcal{U}^\star} J(u_V) \\ J(u_V) &:= a_D(D(T) - D(0)) + a_S(Y_{I_S}(T) - Y_{I_S}(0)) \\ &\text{subject to} \\ f_\lambda &:= \frac{\beta_S I_S + \beta_A I_A}{\widehat{N}} \\ S'(t) &= \mu\widehat{N} - f_\lambda S - (\mu + \psi_V + u_V(t))S + \omega_V V + \sigma_R R \\ E'(t) &= f_\lambda(S + (1-\varepsilon_V)V) - (\mu + \sigma_E)E \\ I_S'(t) &= p\sigma_E E - (\mu + \alpha_S)I_S \\ I_A'(t) &= (1-p)\sigma_E E - (\mu + \alpha_A)I_A \\ R'(t) &= (1-\theta)\alpha_S I_S + \alpha_A I_A - (\mu + \sigma_R)R \\ D'(t) &= \theta\alpha_S I_S \\ V'(t) &= (\psi_V + u_V(t))S - ((1-\varepsilon_V)f_\lambda V + \mu + \omega_V)V \\ X'(t) &= (\psi_V + u_V(t))(S + E + I_A + R) \\ Y_{I_S}'(t) &= p\sigma_E E, \end{aligned} \tag{19}$$

$$\begin{aligned} S(0) &= S_0,\ E(0) = E_0,\ I_S(0) = I_{S_0}, \\ I_A(0) &= I_{A_0},\ R(0) = R_0,\ D(0) = D_0, \\ V(0) &= 0,\ X(0) = 0,\ Y_S(0) = Y_{S_0},\ X(T) = x_{coverage}, \\ u_V(\cdot) &\in [u_{\min}, u^{\max}], \\ \kappa I_S(t) &\le B, \quad \forall t \in [0,T], \\ \widehat{N}(t) &= S + E + I_S + I_A + R + V. \end{aligned}$$

Figure 6 illustrates the main ideas of the above discussion. Table 4 enclose parameter information of the functional cost and constraints.

Existence of solution to our (OCP) in Equation (19) drops in the theory developed by Francis Clark [see e.g. 35, Thm. 23.11]. Since we aim to simulate hypothetical scenarios, we omit here a rigorous proof. Instead, we refer interested readers to [22, 36] and the reference therein.

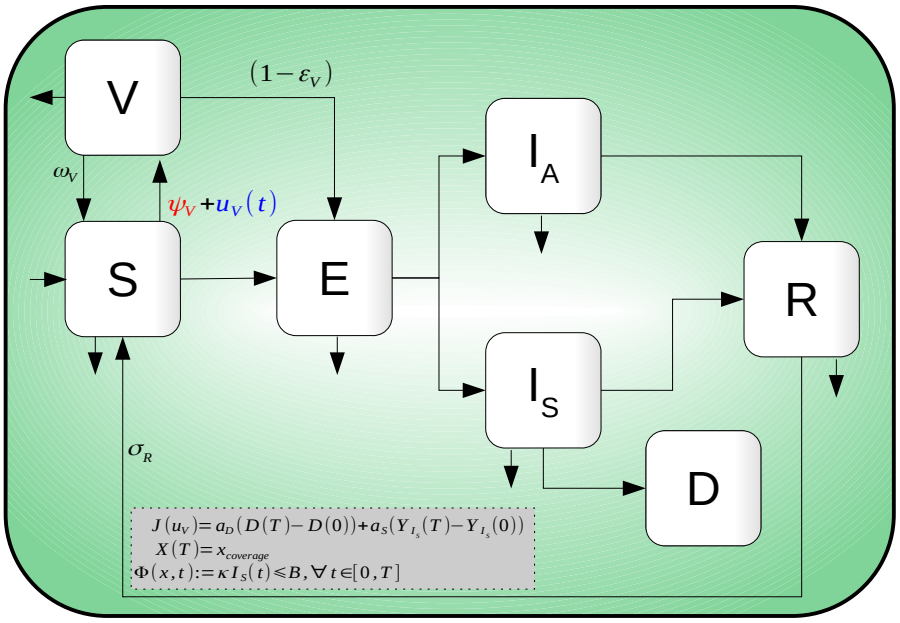

Figure 6: Compartmental diagram of COVID-19 transmission dynamics that includes optimal vaccination dynamics, penalization and a path constraint.

Symbol	Description	Value	Ref
a_D	Penalization weight due to premature mortality (YLL) and estimated from Mexico-City an Mexico-State data	7.5 years	[33, 37]
a_S	Penalization weight due to disability (YLD)	0.008 418 473 years	[34]
$x_{coverage}$	Covering constraint at time horizon T		[1]
κ	Hospitalization rate	0.05	Estimated
B	Health service capacity in number of beds	9500	Estimated

Table 4: Parameters regarding the constraints conditions and cost functional of the OCP (19).

5. Numerical experiments

5.1. Methodology

We apply the so-called transcript method to solve our (OCP). This method transforms the underlying problem of optimizing functional governed by a differential equation into a finite-dimensional optimization problem with restrictions. To fix ideas, let x, u respectively denote state and control, and consider the optimal control problem

$$\begin{aligned}
&\min J(x(\cdot), u(\cdot)) = g_0(T, x(T)) && \text{Functional cost}\\
&\dot{x} = f(t, x(t), u(t)), \quad \forall t \in [0,T], && \text{Dynamics}\\
&u(t) \in \mathcal{U}[0,T] \text{for a.e. } t \in [0,T] && \text{Admissible controls}\\
&g(x(t), u(t)) \leq 0 && \text{Path constrain}\\
&\Phi(x(0), x(T)) = 0 && \text{Boundary conditions.}
\end{aligned}$$

Then, transcription methods transform this infinite-dimensional optimization problem into a finite dimension problem (NLP) via discretization of dynamics, state, and control. For example, if we employ the Euler

method with a discretization of N constant steps with size h, then we can solve

$$\begin{aligned} &\min g_0(t_N, x_N) \\ &x_{i+1} = x_i + hf(x_i, u_i), \quad i = 0, \dots, N-1 \\ &u_i \in \mathcal{U}, \qquad\qquad\qquad i = 0, \dots, N \\ &g(x_i, u_i) \leq 0, \qquad\qquad i = 0, \dots, N \\ &\Phi(x_0, x_N) = 0, \qquad\qquad i = 0, \dots, N, \end{aligned} \tag{20}$$

where $x_i \approx x(t_i)$, $u_i \approx u(t_i)$ in the grid

$$\{t_0 = 0, \quad t_i = ih \ (i = 1, \dots, N-1), \quad t_N = T\}.$$

Let $Y = \{x_0, \dots, x_N, u_0, \dots u_N\}$. Thus Equation (20) defines a nonlinear programming problem on the discretized state and control variables of the form

$$\begin{aligned} &\min F(Y) \\ &\text{such that} \\ &LB \leq C(Y) \leq UB. \end{aligned} \tag{21}$$

The numerical analysis and design of transcript methods is a well established and active research numerical field. There is a vast literature about robust methods and recently, implementations have been developed in vogue languages like Julia [38, 39], Python [40], Matlab [41], and others. We refer the reader to [42, 43] for a more systematic discussion.

Our simulations rely on the `Bocop` package [44, 45] to solve our (OCP). Bocop is part of the development of the INRIA-Saclay initiative for open source optimal control toolbox and supported by the team Commands. BOCOP solves the NLP problem in Equation (21) by the well known software IPOPT and using sparse exact derivatives computed by ADOL-C.

We provide in [46] a GitHub repository with all regarding R and Bocop sources. This repository also encloses data sources and python code to reproduce all reported figures.

5.2. Simulation of hypothetical scenarios

We follow the guidelines reported by the WHO Strategic Advisory Group of Experts (SAGE) on Immunization Working Group on COVID-19 Vaccines modeling questions presented in [1]. According to this SAGE's document, we simulate scenarios to illustrate vaccination policies' response with a preventive vaccine. We aim to contrast the impact of the burden of COVID-19 mitigation regarding

(**SCN**-1) Optimal versus constant vaccination policies
(**SCN**-2) Vaccine efficacy
(**SCN**-3) Induced vaccine immunity
(**SCN**-4) Natural immunity

We consider vaccine profiles—efficacy and induced vaccine immunity—compatible with the firms Pfizer-BioNTech, Moderna, Astra-Zeneca, Gamaleya Research Institute Johnson & Johnson, Sinovac Biotech among others. Further, since reinfection and induced vaccine immunity parameters remain unavailable, we see pertinent to explore the effect of plausible settings. [SDIV 1] cites

Remark 3. Optimal vaccination policy implies that number of doses per unit time described by

$$(\psi_V + u_V(t))(S(t) + E(t) + I_A(t) + R(t))$$

mitigates the outbreak in optimal form, where optimal is defined in terms of function J (see Equation (15)), that is minimizing years of life lost in DALYs. Counterfactual scenarios implies $u_V(t) = 0$. Without vaccination scenarios we means $\psi_V + u_V(t) = 0, \ \forall t \in [0, T]$.

Remark 4. We assume positive prevalence of all epidemiological classes according to the following hypothesis:

(IC)-1 The implemented initial conditions for our numerical experiments are hypothetical and not reflects the actual data reported by Mexico-City and Mexico-State health authorities. The initial conditions are taken such that an outbreak is on its growth phase (see Figure 7).

(IC)-2 We suppose that around of 30 % of the population is under Lockdown and is enclosed along with recovered class R. That is, $R(0)$ encircle mainly children, senior, home office, people with low mobility and COVID-19 recovered individuals.

(IC)-3 Our numerical results are of qualitative nature and non necessarily sustain forecasting or follows the actual profile of the underlying COVID-19 pandemic data.

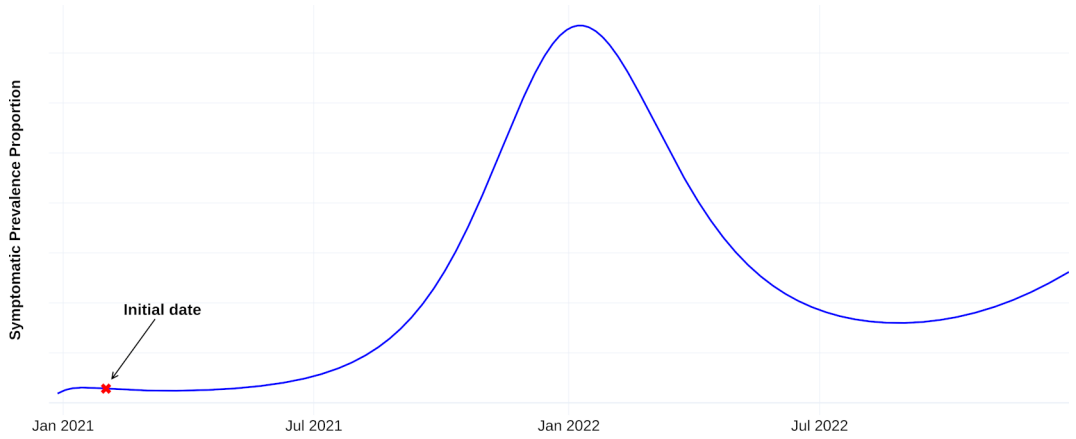

Figure 7: Hypothetical scenario when considering COVID-19 transmission dynamics without vaccination process. Blue line shows symptomatic prevalence dynamics. Red cross represents the initial date of simulations.

Table 5 encloses a brief description and parameter values regarding each scenario. The reader can also access the web `Chart Studio Graph` of each figure regarding data and `plotly` [47] visual representation.

Simulation Scene	**Description**	**Set-up** $(x_{coverage}, T, \varepsilon_V, \omega_V^{-1}, \sigma_R^{-1})$
(SCN-1)	Likening between optimal and constant vaccination policies.	(20 %, 180 days, 70 %, 730 days, lifelong)
(SCN-2)	Vaccine efficacy blow	(50 %, 365 days, {50 %, 70 %, 90 %}, 730 days, 180 days)
(SCN-3)	Induced vaccine immunity period	(50 %, 365 days, 90 %, {180 days, 365 days, 730 days}, 365 days)
(SCN-4)	Natural immunity period	(50 %, 365 days, 90 %, 730 days, {90 days, 180 days, 365 days})

Table 5: Setup parameters for counterfactual and response scenarios. See Table 3 for the rest of parameters.

To perform the simulations corresponding to the scenarios presented in Table 5, we fix the parameter values as in Table 6.

Parameters values		
	(SCN-1)–(SCN4)	
β_S, β_A, α_S, α_A, σ_E, μ, θ, p	Table 3	
a_D, a_S, κ, B	Table 4	
	(SCN-1)	**(SCN-2)–(SCN-4)**
ψ_V	0.001 239 69	0.001 899 03
u_{min}	−0.000 619 845	−0.000 949 52
u_{max}	0.006 198 45	0.004 747 58

Table 6: Fixed parameters values of system in Equation (19).

Optimal Versus Constant Vaccination Policies: (SCN-1)

To fix ideas, we display in Figures 8 and 9 the counterfactual scenario regarding no intervention. We contrast a constant vaccination policy (CP) and optimal vaccination policy (OP) with a vaccine profile of efficacy $\varepsilon_V = 70\,\%$, vaccine-induced immunity $\omega_V^{-1} = 730$ days and a campaign for $20\,\%$ of coverage at 180 days. Figure 8 suggests that the OP improves CP vaccination policy response according to the disease burden due to mortality, and morbidity. Figure 9 confirms this improvement by comparing disease dynamics with and without vaccination. We observe CP and OP reduce disease levels. Although both campaigns administrate the same number of vaccine doses, OP vaccination implies fewer deaths and symptomatic cases. ~~Figure 3 shows a scenario whit $R_0 > 1$. The underlying vaccine reproductive number R_V remains below to R_0. This Figure illustrates the strong relation between disease mitigation, vaccine efficacy (ε_V), and vaccination rate (ψ_V). Further, given a dynamic without vaccine intervention and $R_0 > 1$, R_V projects a minimal vaccination rate to drive this dynamic to the disease-free state but subject to vaccines with particular efficacy.~~

[SDIV 2] Fix th paragraph

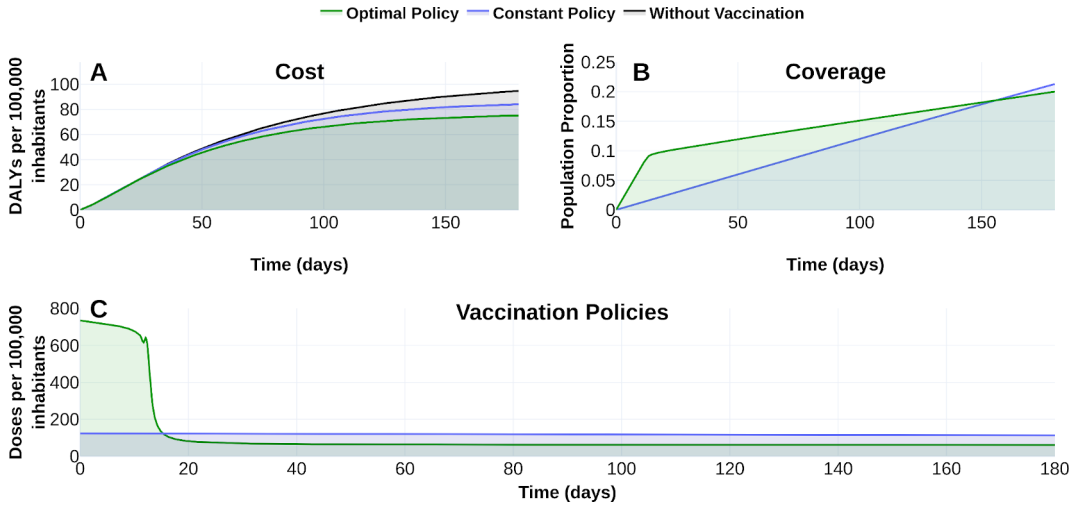

Figure 8: Effect of the vaccination policy on the burden COVID-19 for a 20% coverage at time horizon of half year. (A) Vaccination policies' response regarding constant (ψ_V) and optimal ($\psi_V + u_V(t)$) vaccination rates in the burden of COVID-19 quantified in DALYs. (B) Evolution of the vaccination covering according to each policy. (C) Vaccination schedule for each vaccination policy. Blue translucent color corresponds to policies with constant vaccination rate 0.001 239 69. Green tone is related to the optimal vaccination policy. For counterfactual reference (panel A), black line-gray shade represents the burden of COVID-19 without vaccination. See https://plotly.com/ MAAZ/366/ for plotly visualization and data.

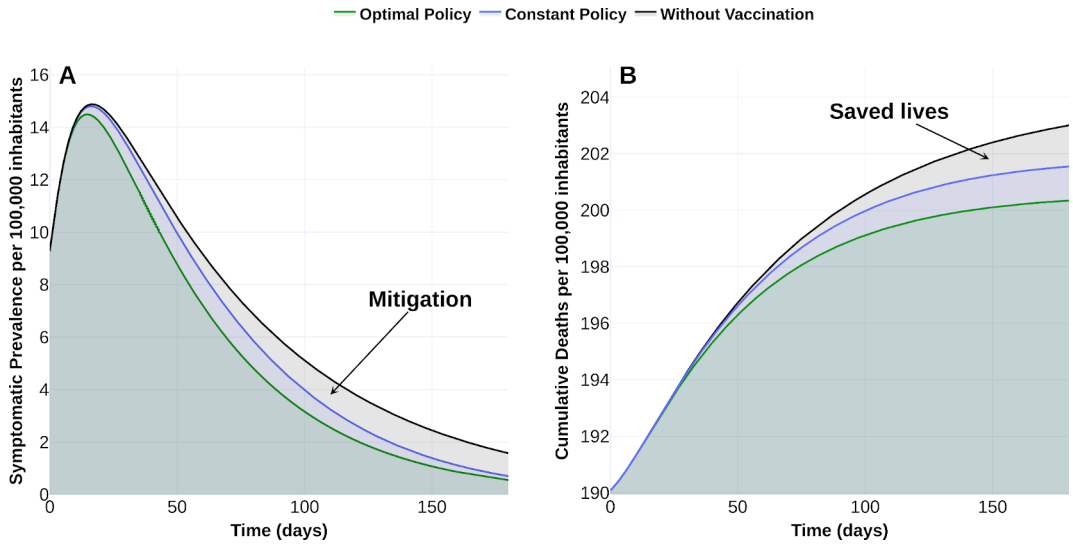

Figure 9: Effect of the vaccination policy on outbreak evolution. (A) Optimal vaccination policy reaches a better response in mitigating symptomatic cases than a policy with a constant vaccination rate. (B) Gray and blue shaded translucent regions denote the number of saved lives per 100 000 inhabitants. The optimal vaccination rate (grey-blue) improves the number of saved lives per 100 000 inhabitants of the constant rate ψ_V. Data and web visualization in https://plotly.com/ MAAZ/370/.

Vaccine Efficacy (SCN-2)

[SDIV 3] Fix. S that has been ap proved develop- ments in Mexico

In February 2021, multiple vaccines have been rolled out to prevent COVID-19 disease. Table 7 contains information on developments that we consider relevant to explore a wide range of plausible vaccine-efficacies.

- by Pfizer-BioNTec has 95% effectiveness (95% CI, 90.3 to 97.6) [50];
- Sputnik V by Gamaleya has 91.6% effectiveness (95% CI 85.6–95.2) [49];

Developer	Vaccine Name	Vaccine Efficacy %, (95% CI)	Reference
Pfizer-BioNTech	BNT162b2	95 (90.3–97.6)	[48]
Gamaleya Institute	Sputnik V	91.6 (85.6–95.2)	[49]
Oxford University-AztraZeneca	AZD1222	74.6 (41.6-88.9)	[5]
Johnson & Johnson	Ad26.COV2.S	72 %	[6]
Sinovac Biotech	CoronaVac	50.4%	[48]

Table 7: Vaccine efficacy of some to the platforms approved to emergency use.

- AZD1222 by Oxford-48AstraZeneca has vaccine efficacy for different virus lineages with 74.6% [95% CI 41.6-88.9] and 84 % [95% CI 70.7-91.4], respectively [5];
- Ad26.COV2.S by Johnson & Johnson has a vaccine's efficacy against moderate and severe disease ranged from one country to another: 72% in the US, 66% in Latin America and 57% in South Africa [6];
- CoronaVac by Sinovac Biotech has 50.4% effectiveness [48].

Figures 10 and 11 display the optimal vaccination policy's response according to three vaccines with different efficacy. Figure 10A displays COVID-19 burden in DALYs for policies with 50 %, 70 %, 90 % vaccine-efficacies. Figures 10B-C also illustrate the effect of vaccine-efficacies on coverage and optimal vaccination policy respectively. We observe that vaccine-efficacy influences design optimal policy. According to 50 % coverage at a time horizon of 1 year, Figure 11 displays an improvement of at least three times in the prevalence of symptomatic cases and saved lives concerning the uncontrolled outbreak. Figure 11 reflects this effect in the mitigation symptomatic prevalence (A) and the number of saved lives (B) shaded by the translucent grey (50% vaccine efficacy), grey-blue (70% vaccine efficacy), and grey-blue-red (90% vaccine efficacy).

[SDIV 4] how?, be concise

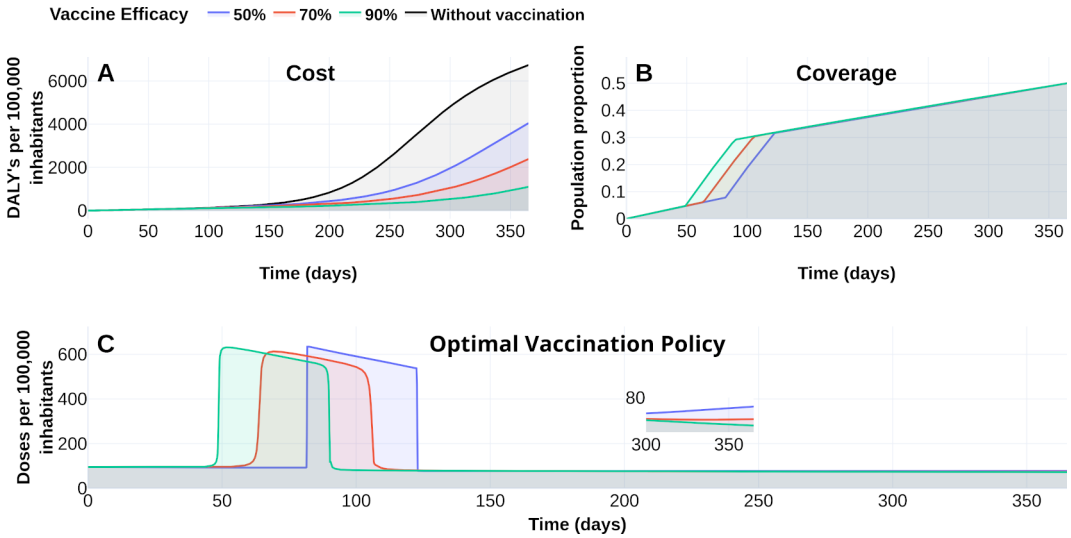

Figure 10: The response of COVID-19 burden to vaccine efficacy. (A) COVID-19 burden response quantified in DALYs per 100 000 inhabitants to vaccines with efficacy of 50 % (blue), 70 % (red) and 90 %(green). (B) Coverage evolution to reach 50 % of the total population vaccinated. (C) Optimal vaccination doses schedule according to the different efficacies. See https://plotly.com/ MAAZ/358/ for visualization and data.

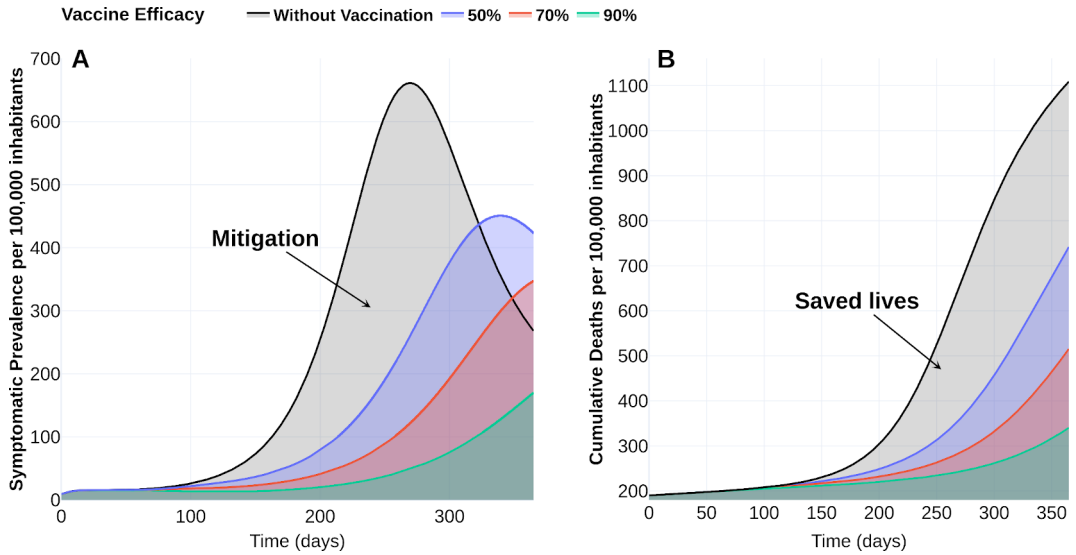

Figure 11: The effect of vaccine efficacy over COVID-19 symptomatic prevalence and morbidity. (A) Effect of vaccine-efficacy of 50 % (blue), 70 % (red) and 90 % (green) on prevalence of symptomatic cases per 100 000 inhabitants. (B) Effect of vaccine-efficacy on the number of saved lives. See https://plotly.com/ MAAZ/375/ for data and visualization.

Vaccine-induced immunity (SCN-3)

Vaccine response also is strongly related to its induced immunity —parameter that remains poorly understood [3]. Here, we contrast two vaccines with different induced-immunity. Let denote by vax_1, vax_2, vax_3 vaccines with an induced-immunity capacity of a half, one, and two years, respectively, and common efficacy of 90 %. Consider a vaccine camping of time horizon of one year and 50 % coverage. Taking the same dynamics parameters, that is initial conditions, and baseline parameters, as in Table 3, we explore a counterfactual scenario with an uncontrolled outbreak of $R_0 = 1.794\,93$ and three controlled dynamics according to vaccines vax_1, vax_2, vax_3. Thus, according to these immunity parameters and factor defined in **??**, respectively, results $R_V^{[vax_1]} = 1.385\,55$, $R_V^{[vax_2]} = 1.139\,13$, $R_V^{[vax_3]} = 0.867\,56$ for vaccine immunities periods of a half, one, and two years. We display in Figure 12 the response of the vaccines vax_1, vax_2 and vax_3. *Since optimal vaccination policies are similar, Figure 12 A suggests vaccine-induced immunity rate is not determinant in the vaccination schedule design.* ~~*Since in this scenario set time horizon is of one year, the optimal policies follow similar schedules and imply similar gains in the number of years of life lost. Despite these similarities,*~~ Figure 13 displays ~~*in panel A dramatically gain respect to*~~ *a wide reduction of disease levels concerning the uncontrolled outbreak.* ~~*—since $R_V^{[vax_2]}$ is near to one, prevalence fall down more than five times and because $R_V^{[vax_3]}$ is less that one, prevalence of symptomatic cases tends to zero with damped oscillations. Figure 13 also endorses this gain regarding saved lives (B). This gain is*~~ *It happens as a consequence of the vaccine reproduction number reductions. For this scenario, we observe that it is unnecessary to reduce R_V below one to obtain notable mitigation. The disease level reduction represented by the shaded grey region (a half year), grey-green region (one years) and grey-green-red region (two years).*

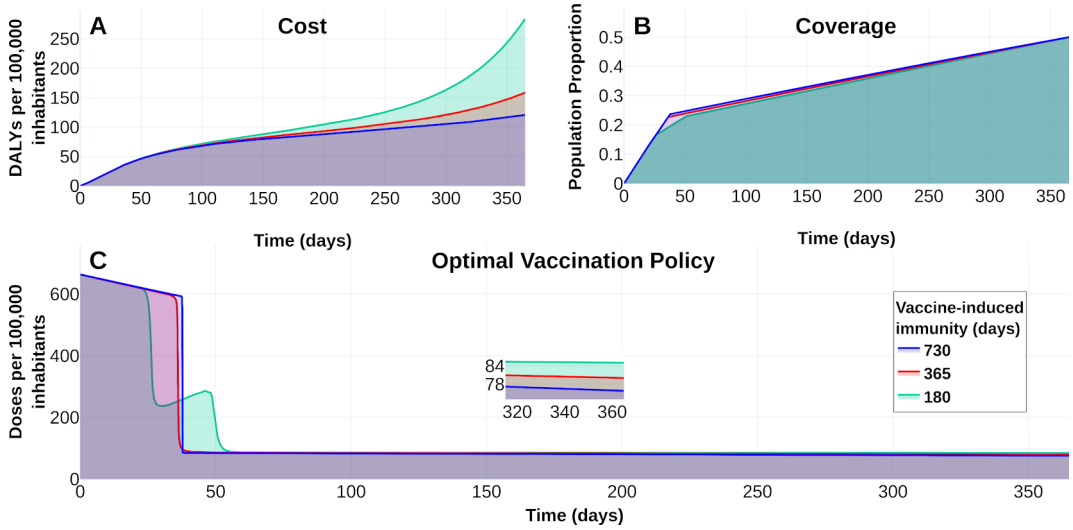

Figure 12: Effect of vaccine-induced immunity on the COVID-19 burden. (A) Effect on the burden of COVID-19 quantified in DALYs per 100 000 inhabitants due to vaccine-induced immunity of 180 days (green), 365 days (red) and 730 days (blue). (B) Coverage evolution to reach 50 % of the total population vaccinated. (C) Optimal vaccination doses schedule according to the different vaccine-induced immunities. Visualization and data in https://plotly.com/ MAAZ/407/ .

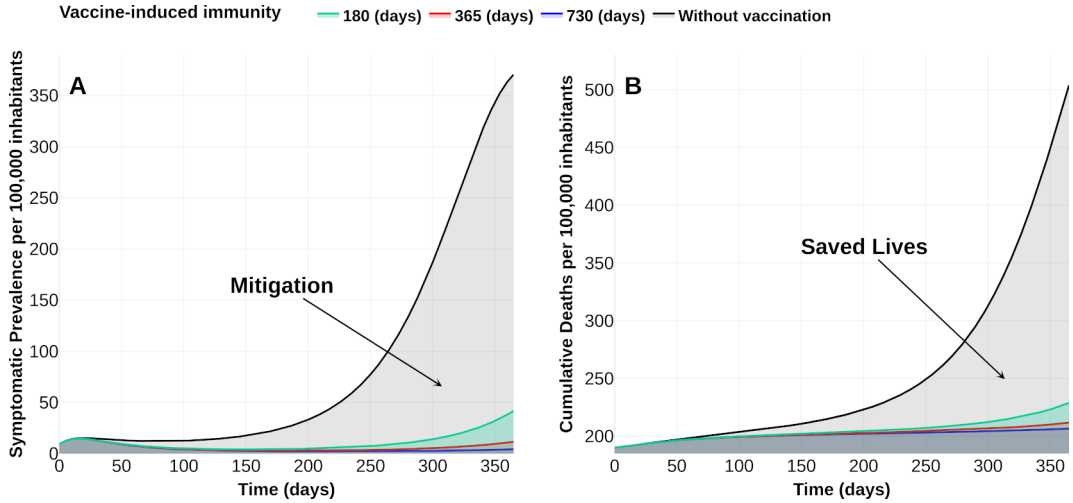

Figure 13: Effect of vaccine-induced immunity on mitigation and saved lives of COVID-19 outbreak. (A) Effect of vaccine-induced immunity on mitigation of symptomatic prevalence per 100 000 inhabitants. (B) The number of saved lives. See https://plotly.com/ MAAZ/416/.

Natural Immunity Hypothesis (SCN-4)

"Reinfections raise questions about long-term immunity to COVID-19 and the prospects for a vaccine", reported Heidi Ledford in [51]. Following this line, we display in Figures 14 and 15 the vaccine's response with 90 % efficacy and contrasting with natural immunity periods of 90 days, 180 days, and 365 days. Here, the adjective "natural" denotes the immunity that an individual develops after recovering from a previous bout of COVID-19 without vaccination. When implementing an optimal vaccination strategy, if natural immunity lasts one year, the burden of COVID-19 falls until around 120 DALYs. We confirm this behavior in the prevalence of symptomatic cases and cumulative deaths, as displayed in Figure 15. When natural immunity is 365 days, the gain in mitigation concerning a natural immunity of 90 days is at least 100 times, while the number of deaths with a natural immunity of 90 days reach 845 cases per 100 000 inhabitants, in contrast, of 206 when natural immunity is 365 days. Thus, this simulation suggests that natural immunity plays a vital role in the controlled outbreak's behavior, which is consistent with the conclusions reported in [3].

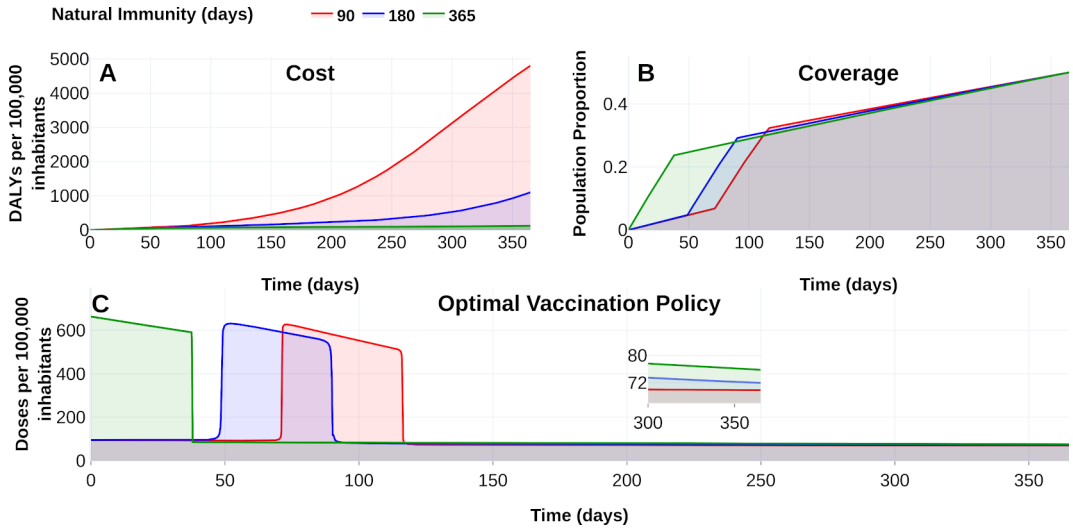

Figure 14: Effect of natural immunity on the burden of COVID-19. (A) Effect on the burden of COVID-19 quantified in DALYs per 100,000 inhabitants due to natural immunity of 90 days (red), 180 days (blue) and 365 days (green). (B) Coverage evolution to reach 50 % of the total population vaccinated. (C) Optimal vaccination doses schedule according to the different natural immunities. See https://plotly.com/ MAAZ/402/.

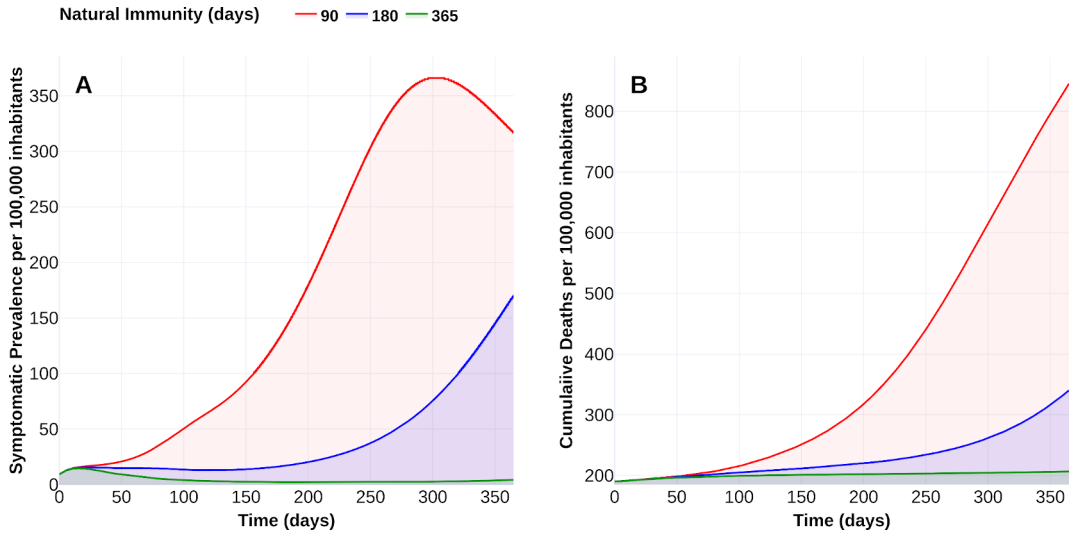

Figure 15: Effect of natural immunity on mitigation and saved lives of COVID-19 outbreak. (A) Effect of immunity on mitigation of symptomatic prevalence per 100 000 inhabitants. (B) Number of saved lives. Plotly visualization and data in https://plotly.com/ MAAZ/406/ .

6. Discussion

In February 2021, at least four vaccination developments support the primary pharmaceutical measure to recover life's style before the pandemic. Although the leading pharmaceutics firms report high vaccine efficacy, its implementation implies new challenges as its distribution, stocks, politics, logistic, among others, emerge. A fair distribution and application strategy is imperative to manage the available resources. Despite that vaccine-immunization response remains under study, vaccination campaigns recently tarted. Thus evaluating the impact of different vaccine profiles and natural immune responses would be crucial to calibrate vaccination policies. Further, since the vaccine doses are scarce at the beginning of the COVID-19 vaccination campaigns optimize their administration subject to its availability, minimizing deaths, and preserving health systems is mandatory.

We aim to compare different vaccine profiles in computing optimal vaccination policies for COVID-19 and evaluate the impact of hypothetical reinfection and immunization responses. Our simulations suggest that an optimal strategy design is influenced by vaccine profile and natural immunity period. Likewise, we observe that natural and vaccine-induced immunity would play an essential role in reducing COVID-19 disease mortality and prevalence levels. Poland et al. [52] stress that understanding immune responses to SARS-CoV-2 are crucial to developing vaccines. Our simulation faces different vaccine-induced and natural immunization profiles, allowing the study of these variables' effects and developing optimal dose administration schedules. Further, our optimal solution satisfies modeling constraints to obtain the desired vaccination coverage and avoid health system overload. We optimized vaccination strategies by minimizing the COVID-19 burden quantified in DALYs. Note that the elderly population has been the most affected in terms of deaths due to the disease. We computed DALYs considering only this population. Stratification becomes important when vaccination strategies prioritize risk groups to reduce burden. Although our model lacks an age-stratified structure, these results would apply to situations where the population has homogeneous characteristics. This kind of population's designs arises, for example, in places like factories, offices, or even schools. The question "who vaccinate first?" has been faced as an optimalallocation problem in [23–25]. The solutions presented here have a complementary objective to the optimal policies offered these preprints—our contribution answers when and how to administrate vaccine doses, while the mentioned references answer who vaccinate first.

In [29] the authors answered when to vaccinate optimally. They used a signal that switches between not vaccination and immunization of all susceptible individuals. Since the vaccine is scarce, this control signal

would be unrealistic in some situations. Our results improve this strategy by modulating a base vaccination rate in a more realistic bound. Further, we consider more detailed dynamics: our model includes exposed and dead classes and differences between symptomatic infectious kinds.

We relate vaccination rate with the available vaccine stock and health system response—limited by logistics, management, politics, and other issues related to each vaccine development. So, our contribution can help decision-makers to design vaccination schedules of homogeneous populations.

When writing this article, the vaccine-induced immunity period and SARS-CoV-2 transmission capacity from a vaccinated individual remain unexplained. [52]. The conclusive answer inevitably will drive the development of COVID-19 vaccines and their policies. Experts estimate that around 7 800 billion immunization doses are required to reach herd immunity. This number, with the approved developments, is far away to accomplish in one year. However, we expect that more vaccines finish their third trial phase and also get approval. Thus, vaccination policies also have to contemplate two o more vaccine profiles, perhaps with different efficacy o number of recommended doses.

These issues also have to balance the health services and other resources optimally.

7. Conclusions

At the date of writing this article, humankind lacks strategies to eradicate COVID-19. Although NPIs implemented in most countries prevent citizens from being infected, these strategies leave them susceptible—people can not develop immunity to face futures waves. Thus, vaccination becomes the primary pharmaceutical measure to recover life's style before the pandemic. However, this vaccine has to be effective and well implemented in global vaccination programs. Thus new challenges as its distribution, stocks, politics, vaccination efforts, among others, emerge. A fair distribution and application strategy is imperative to manage the available resources, especially in developing countries.

We established an optimal control problem to design vaccination strategies where vaccination modulates dynamics susceptibility through an imperfect vaccine. We aimed to provide vaccination policies that minimize the lost life years due to disability or premature death by COVID-19, determined by cumulative deaths and cumulative incidence. Policies' acts in the minimization of infected people's prevalence and the number of deaths.

Our simulations suggest a better response with optimal vaccination policies than policies with a constant vaccination rate. For example, the optimal policy schedule in scenario **SCN-1** increases the number of doses in the scheme's initial stage. This vaccination scheme improves the mitigation of the symptomatic prevalence, the incidence of deaths, and in consequence, the years of life lost quantified in DALYs.

Emerging press releases reported that Pfizer's, Russian Sputnik V, and Moderna's coronavirus vaccines reach efficacy over 90 % [53–55]. However, this information remains under development. Thus vaccine efficacy scenarios of 50 %, 70 %, and 90 % **(SCN-2)** illustrate the effect on optimal vaccination policies' schedule by pointing when to intensify the number of doses. According to the time horizon of one year and coverage of 50%, our numerical experiments suggest that 90 % vaccine efficacy reduces around three times the number of deaths regarding the dynamics without vaccination. Likewise, these vaccines reach a gain of eighteen times in the years of life lost compared to the without vaccination scenario.

Our numerical experiments also illustrate vaccine-induced immunity's relation between the reproductive vaccination number R_V and vaccination policies **(SCN-3)**. Considering an outbreak with a reproductive number R_0 of 1.794 93, vaccine-induced immunity of 365 or 730 days implies a reduction of R_0—dropping its value respectively to 1.139 130 and 0.867 56. Likewise, optimal policies linked to vaccine-induced immunities enhance symptomatic prevalence mitigation and the number of saved lives. Moreover, according to the initial number of deaths, the scenario without vaccination accumulates 503 deads compared to 211 and 206 deads of the underlying dynamics with vaccine-induced immunities.

Barbosa et al. recently report in [29] a simpler model about modeling of COVID-19 vaccination with a similar approach. Although they establish a less detailed model —they do not distinguish between symptomatic and asymptomatic infected individuals—its control problem return policies according to multi-objective policies. Their optimal policy is pragmatic but, in our opinion, not necessarily practical for large

populations. Further, our model extends the result of [29] by a more detailed vaccine profile. Thus we can evaluate how vaccine efficacy, vaccine-induced, and natural immunity parameters impact the mitigation of an optimal vaccination schedule.

Perkins and España report in [27] a vaccination model with optimal control, but they approach to optimize the NPIs. The methodology presented here is similar, but aim very different. However, we want to stress the relevance of also including NPIs effects.

Since any vaccine's efficacy will be subject to uncertainty and immunization regarding COVID-19 remains under development, policymakers need better modeling tools to design fair vaccination programs. We faced this problem by simulation.

According to DALYs definition, segregation as age, comorbidities, and other risk groups is imperative to design more realistic vaccination policies. Moreover, it is well-known that various vaccines platforms and strategies are developing in parallel, and the most recent advance is with vaccines that require two doses. From [27], we can deduce that NPIs, together with vaccination, would constitute a better description of COVID-19 control. We will direct our attention to extend this work according to the segregation and optimization of NPIs-vaccination controls.

Data availability

All code is available at
https://github.com/SaulDiazInfante/ NovelCovid19-ControlModelling/ tree/master/
UNISON-ITSON-VACCINATON-PRJ

Authors' contributions

The first and second authors named are leads. The second named author is the corresponding author. All other authors are listed in alphabetical order.

Manuel Adrian Acuña-Zegarra: Conceptualization, Methodology, Software, Validation, Formal analysis, Investigation, Resources, Visualization, Project Administration, Writing–original draft, Writing–review & editing, Funding acquisition.

Saul Diaz-Infante: Conceptualization, Methodology, Software, Validation, Formal analysis, Investigation, Data curation, Visualization, Supervision, Writing–original draft, Writing–review & editing.

David Baca Carrasco: Conceptualization, Methodology, Formal analysis, Writing–original draft, Writing–review & editing, Funding acquisition.

Daniel Olmos Liceaga: Conceptualization, Methodology, Formal analysis, Formal analysis, Writing–original draft, Writing–review & editing.

Acknowledgments

The authors acknowledge support from grant DGAPA-PAPIIT IV100220 and the Laboratorio Nacional de Visualización Científica UNAM. MAAZ acknowledges support from PRODEP Programme (No. 511-6/2019-8291). DBC acknowledges support from PRODEP Programme (No. 511-6/2019-8022). We thank Dr. Jorge X. Velasco-Hernandez for useful comments and discussions of this work.

Conflicts of interest

The authors have no competing interests.

References

[1] World Health Organization, Strategic Advisory Group of Experts (SAGE) on Immunization Working Group on COVID-19 Vaccines: WHO Strategic Advisory Group of Experts (SAGE), 2020. URL: https://www.who.int/immunization/policy/sage/SAGE_WG_COVID19_Vaccines_Modelling_Questions_31July2020.pdf?ua=1.

[2] C. Gaebler, Z. Wang, J. C. C. Lorenzi, F. Muecksch, S. Finkin, M. Tokuyama, et al., Evolution of antibody immunity to SARS-CoV-2, Nature (2021). doi:10.1038/s41586-021-03207-w.

[3] M. Jeyanathan, S. Afkhami, F. Smaill, M. S. Miller, B. D. Lichty, Z. Xing, Immunological considerations for COVID-19 vaccine strategies, Nature Reviews Immunology 20 (2020) 615–632. doi:10.1038/s41577-020-00434-6.

[4] C. Rydyznski Moderbacher, S. I. Ramirez, J. M. Dan, A. Grifoni, K. M. Hastie, D. Weiskopf, S. Belanger, R. K. Abbott, C. Kim, J. Choi, Y. Kato, E. G. Crotty, C. Kim, S. A. Rawlings, J. Mateus, L. P. V. Tse, A. Frazier, R. Baric, B. Peters, J. Greenbaum, E. Ollmann Saphire, D. M. Smith, A. Sette, S. Crotty, Antigen-Specific Adaptive Immunity to SARS-CoV-2 in Acute COVID-19 and Associations with Age and Disease Severity, Cell 183 (2020) 996–1012.e19. doi:10.1016/j.cell.2020.09.038.

[5] K. R. W. Emary, T. Golubchick, P. K. Aley, C. V. Ariani, B. J. Angus, S. Bibi, B. Blane, D. Bonsall, P. Cicconi, S. Charlton, E. Clutterbuck, A. Collins, T. Cox, T. Darton, et. al., Efficacy of ChAdOx1 nCoV-19 (AZD1222) Vaccine Against SARS-CoV-2 VOC 202012/01 (B.1.1.7), The Lancet (2021). doi:10.2139/ssrn.3779160.

[6] Johnson & Johnson, Johnson & Johnson Announces Single-Shot Janssen COVID-19 Vaccine Candidate Met Primary Endpoints in Interim Analysis of its Phase 3 ENSEMBLE Trial, 2021. URL: https://www.jnj.com/johnson-johnson-announces-single-shot-janssen-covid-19-vaccine-candidate-met-primary-endpoints-in-interim-analysis-of-i accessed February 15, 2021.

[7] E. Toner, A. Barnill, C. Krubiner, J. Benstein, L. Privor-Dumm, M. Watson, Interim framework for covid-19 vaccine allocation and distribution in the united states. august 2020. johns hopkins bloomberg school of public health, Center for Health Security (2020). URL: https://www.centerforhealthsecurity.org/our-work/pubs_archive/pubs-pdfs/2020/200819-vaccine-allocation.pdf.

[8] E. A. Iboi, C. N. Ngonghala, A. B. Gumel, Will an imperfect vaccine curtail the COVID-19 pandemic in the U.S.?, Infectiuos disease modelling 5 (2020) 510–524. doi:10.1016/j.idm.2020.07.006.

[9] A. B. Gumel, E. A. Iboi, C. N. Ngonghala, N. G. A., Mathematical assessment of the roles of vaccination and non-pharmaceutical interventions on COVID-19 dynamics: a multigroup modeling approach, medRxiv (2020). doi:10.1101/2020.12.11.20247916.

[10] M. Makhoul, H. H. Ayoub, H. Chemaitelly, S. Seedat, G. R. Mumtaz, S. Al-Omari, L. J. Abu-Raddad, Epidemiological Impact of SARS-CoV-2 Vaccination: Mathematical Modeling Analyses, Vaccines 8 (2020) 1–16. doi:10.3390/vaccines8040668.

[11] M. Liu, J. Ning, Y. Du, J. Cao, D. Zhang, J. Wang, M. Chen, Modelling the evolution trajectory of COVID-19 in Wuhan, China: experience and suggestions, Public Health 183 (2020) 76–80. doi:10.1016/j.puhe.2020.05.001.

[12] K. Sarkar, S. Khajanchi, J. J. Nieto, Modeling and forecasting the COVID-19 pandemic in India, Chaos, Solitons and Fractals 139 (2020) 110049 (1–16). doi:10.1016/j.chaos.2020.110049.

[13] M. A. Capistran, A. Capella, J. A. Christen, Forecasting hospital demand in metropolitan areas during the current COVID-19 pandemic and estimates of lockdown-induced 2nd waves, PLOS ONE 16 (2021) e0245669. URL: https://dx.plos.org/10.1371/journal.pone.0245669. doi:10.1371/journal.pone.0245669.

[14] H. J. T. Unwin, S. Mishra, V. C. Bradley, A. Gandy, T. A. Mellan, H. Coupland, J. Ish-Horowicz, M. A. C. Vollmer, C. Whittaker, S. L. Filippi, X. Xi, M. Monod, O. Ratmann, M. Hutchinson, F. Valka, H. Zhu, I. Hawryluk, P. Milton, K. E. C. Ainslie, M. Baguelin, A. Boonyasiri, N. F. Brazeau, L. Cattarino, Z. Cucunuba, G. Cuomo-Dannenburg, I. Dorigatti, O. D. Eales, J. W. Eaton, S. L. van Elsland, R. G. FitzJohn, K. A. M. Gaythorpe, W. Green, W. Hinsley, B. Jeffrey, E. Knock, D. J. Laydon, J. Lees, G. Nedjati-Gilani, P. Nouvellet, L. Okell, K. V. Parag, I. Siveroni, H. A. Thompson, P. Walker, C. E. Walters, O. J. Watson, L. K. Whittles, A. C. Ghani, N. M. Ferguson, S. Riley, C. A. Donnelly, S. Bhatt, S. Flaxman, State-level tracking of COVID-19 in the United States, Nature Communications 11 (2020) 6189. URL: http://dx.doi.org/10.1038/s41467-020-19652-6http://www.nature.com/articles/s41467-020-19652-6. doi:10.1038/s41467-020-19652-6.

[15] M. A. Acuña-Zegarra, M. Santana-Cibrian, J. X. Velasco-Hernandez, Modeling behavioral change and COVID-19 containment in Mexico: A trade-off between lockdown and compliance, Mathematical Biosciences 325 (2020) 108370. doi:10.1016/j.mbs.2020.108370.

[16] M. Santana-Cibrian, M. A. Acuña-Zegarra, J. X. Velasco-Hernandez, Lifting mobility restrictions and the effect of superspreading events on the short-term dynamics of COVID-19, Mathematical Biosciences and Engineering 17 (2020) 6240–6258. doi:10.3934/mbe.2020330.

[17] M. R. Tocto-Erazo, J. A. Espíndola-Zepeda, J. A. Montoya-Laos, M. A. Acuña-Zegarra, D. Olmos-Liceaga, P. A. Reyes-Castro, G. Figueroa-Preciado, Lockdown, relaxation, and acme period in COVID-19: A study of disease dynamics in Hermosillo, Sonora, Mexico, PloS ONE 15 (2020) e0242957. doi:10.1371/journal.pone.0242957.

[18] C. N. Ngonghala, E. Iboi, S. Eikenberry, M. Scotch, C. R. MacIntyre, M. H. Bonds, A. B. Gumel, Mathematical assessment of the impact of non-pharmaceutical interventions on curtailing the 2019 novel Coronavirus, Mathematical Biosciences 325 (2020) 108364. doi:10.1016/j.mbs.2020.108364.

[19] A. S. Shaikh, I. N. Shaikh, K. S. Nisar, A mathematical model of COVID-19 using fractional derivative: outbreak in India with dynamics of transmission and control, Advances in Difference Equations 373 (2020) 1–19. doi:10.1186/s13662-020-02834-3.

[20] A. De Visscher, The COVID-19 pandemic: model-based evaluation of nonpharmaceutical interventions and prognoses, Nonlinear Dynamics 101 (2020) 1871–1887. doi:10.1007/s11071-020-05861-7.
[21] J. S. Weitz, S. J. Beckett, A. R. Coenen, D. Demory, M. Dominguez-Mirazo, J. Dushoff, C. Y. Leung, G. Li, A. Măgălie, S. W. Park, R. Rodriguez-Gonzalez, S. Shivam, C. Y. Zhao, Modeling shield immunity to reduce COVID-19 epidemic spread, Nature Medicine 26 (2020) 849–854. URL: https://doi.org/10.1038/s41591-020-0895-3. doi:10.1038/s41591-020-0895-3.
[22] S. Lenhart, J. T. Workman, Optimal control applied to biological models, Chapman & Hall/CRC Mathematical and Computational Biology Series, Chapman & Hall/CRC, Boca Raton, FL, 2007. doi:10.1201/9781420011418.
[23] L. Matrajt, J. Eatontra, T. Leung, E. R. Brown, Vaccine optimization for COVID-19, who to vaccinate first?, medRxiv (2020). doi:10.1101/2020.08.14.20175257.
[24] K. M. Bubar, K. Reinholt, S. M. Kissler, M. Lipsitch, S. Cobey, Y. H. Grad, D. B. Larremore, Model-informed COVID-19 vaccine prioritization strategies by age and serostatus, MedRxiv (2020). doi:10.1101/2020.09.08.20190629.
[25] J. H. Buckner, G. Chowell, M. R. Springborn, Optimal Dynamic Prioritization of Scarce COVID-19 Vaccines, medRxiv (2020). doi:10.1101/2020.09.22.20199174.
[26] C. E. Madubueze, S. Dachollom, I. O. Onwubuya, Controlling the Spread of COVID-19: Optimal Control Analysis, Computational and Mathematical methods in Medicine 2020 (2020) 6862516(1–14). doi:10.1155/2020/6862516.
[27] T. A. Perkins, G. España, Optimal Control of the COVID-19 Pandemic with non-pharmaceutical Interventions, Bulletin of Mathematical Biology 82 (2020) 118(1–24). doi:10.1007/s11538-020-00795-y.
[28] S. Ullah, M. A. Khan, Modeling the impact of non-pharmaceutical interventions on the dynamics of novel coronavirus with optimal control analysis with a case study, Chaos, Solitons and Fractals 139 (2020) 110075(1–15). doi:10.1016/j.chaos.2020.110075.
[29] G. Barbosa Libotte, F. Sérgio Lobato, G. Mendes Platt, A. J. Silva Neto, Determination of an optimal control strategy for vaccine administration in COVID-19 pandemic treatment, Computer Methods and Programs in Biomedicine 196 (2020) 105664(1–13). doi:10.1016/j.cmpb.2020.105664.
[30] P. Van den Driessche, J. Watmough, Reproduction numbers and sub-threshold endemic equilibria for compartmental models of disease transmission, Mathematical Biosciences 180 (2002) 29–48. doi:10.1016/S0025-5564(02)00108-6.
[31] M. E. Alexander, C. Bowman, S. M. Moghadas, R. Summers, A. B. Gumel, B. M. Sahai, A vaccination model for transmission dynamics of influenza, SIAM Journal on Applied Dynamical Systems 3 (2004) 503–524. doi:10.1137/030600370.
[32] H. Tian, Y. Liu, Y. Li, C.-H. Wu, B. Chen, M. U. Kraemer, B. Li, J. Cai, B. Xu, Q. Yang, et al., An investigation of transmission control measures during the first 50 days of the COVID-19 epidemic in China, Science 368 (2020) 638–642. doi:10.1126/science.abb6105.
[33] World of Health Organization, WHO methods and data sources for global burden of disease estimates 2000-2011, Accessed 2020. URL: https://www.who.int/healthinfo/statistics/GlobalDALYmethods_2000_2011.pdf.
[34] M. W. Jo, D. S. Go, R. Kim, S. W. Lee, M. Ock, Y. E. Kim, I. H. Oh, S. J. Yoon, H. Park, The Burden of Disease due to COVID-19 in Korea Using Disability-Adjusted Life Years, Journal of Korean Medical Science 35 (2020) e199 (1–10). doi:10.3346/jkms.2020.35.e199.
[35] F. Clarke, Functional analysis, calculus of variations and optimal control, volume 264 of *Graduate Texts in Mathematics*, Springer, London, 2013. doi:10.1007/978-1-4471-4820-3.
[36] R. F. Hartl, S. P. Sethi, R. G. Vickson, A survey of the maximum principles for optimal control problems with state constraints, SIAM Rev. 37 (1995) 181–218. doi:10.1137/1037043.
[37] Gobierno de México, Datos abiertos, https://www.gob.mx/salud/documentos/datos-abiertos-152127, 2020 (Accessed November 10, 2020).
[38] I. Dunning, J. Huchette, M. Lubin, Jump: A modeling language for mathematical optimization, SIAM Review 59 (2017) 295–320. doi:10.1137/15M1020575.
[39] M. Lubin, I. Dunning, Computing in operations research using julia, INFORMS Journal on Computing 27 (2015) 238–248. doi:10.1287/ijoc.2014.0623.
[40] E. Benazera, N. Hansen, libcmaes documentation, 2020. URL: https://github.com/beniz/libcmaes/wiki.
[41] Mathworks, fmincon interior point algorithm, 2020. URL: https://www.mathworks.com/help/optim/ug/constrained-nonlinear-optimization-algorithms.html#brnpd5f.
[42] J. T. Betts, Practical Methods for Optimal Control Using Nonlinear Programming, Third Edition, Society for Industrial and Applied Mathematics, Philadelphia, PA, 2020. URL: https://doi.org/10.1137/1.9781611976199.
[43] H. Seywald, E. M. Cliff, Goddard problem in presence of a dynamic pressure limit, Journal of Guidance, Control, and Dynamics 16 (1993) 776–781. doi:10.2514/3.21080.
[44] I. S. Team Commands, Bocop: an open source toolbox for optimal control, http://bocop.org/download/, 2017.
[45] J. Bonnans, Frederic, D. Giorgi, V. Grelard, B. Heymann, S. Maindrault, P. Martinon, O. Tissot, J. Liu, Bocop – A collection of examples, Technical Report, INRIA, 2017. URL: http://www.bocop.org/examples-2/.
[46] S. Diaz-Infante, A. Acuña-Zegarra, D. Baca-Carrasco, D. Olmos-Liceaga, Source code for the manuscript Optimal Vaccine Policies for COVID-19, 2020. URL: https://github.com/SaulDiazInfante/NovelCovid19-ControlModelling/tree/master/UNISON-ITSON-VACCINATON-PRJ.
[47] Plotly Technologies Inc., Collaborative data science, 2015. URL: https://plot.ly.
[48] New York Times, Coronavirus Vaccine Tracker, 2020. URL: https://www.nytimes.com/interactive/2020/science/coronavirus-vaccine-tracker.html?auth=login-google1tap&login=google1tap, accessed January 20, 2021.
[49] D. Y. Lugonov, I. V. Dolzhikova, D. V. Shcheblyakov, A. I. Tukhvatulim, O. V. Zubkuva, A. S. Dzharullaeva, A. V. Kovyrshina, N. L. Lubenets, D. M. Grousova, A. S. Erohova, A. G. Botikov, O. Izhaeva, F. M. Popova, T. A. Ozharovskaya, I. B. Esmagambetov, I. A. Favorskaya, D. I. Zrelkin, D. V. Voronina, Safety and efficacy of an rAd26 and rAd5 vector-

based heterologous prime-boost COVID-19 vaccine: an interim analysis of a randomised controlled phase 3 trial in Russia, The Lancet (2021). doi:10.1016/S0140-6736(21)00234-8.
[50] F. P. Polack, S. J. Thomas, N. Kitcin, J. Absalon, A. Gurtman, S. Lockhart, J. L. Perez, G. Pérez Marc, E. D. Moreira, C. Zerbini, R. Bailey, K. A. e. a. Swanson, Safety and Efficacy of the BNT162b2 mRNA Covid-19 Vaccine, The New England Journal of Medicine 383 (2020) 2603–2615. doi:10.1056/NEJMoa2034577.
[51] H. Ledford, Coronavirus reinfections: three questions scientists are asking, Nature 585 (2020) 168–169. doi:10.1038/d41586-020-02506-y.
[52] G. A. Poland, I. G. Ovsyannikova, R. B. Kennedy, SARS-CoV-2 immunity: review and applications to phase 3 vaccine candidates, The Lancet 396 (2020) 1595–1606. URL: https://doi.org/10.1016/https://linkinghub.elsevier.com/retrieve/pii/S0140673620321371. doi:10.1016/S0140-6736(20)32137-1.
[53] N. Kounang, Pfizer says early analysis shows its Covid-19 vaccine is more than 90% effective, 2020. URL: https://edition.cnn.com/2020/11/09/health/pfizer-covid-19-vaccine-effective/index.html, prees release.
[54] P. Ivanova, Russia says its sputnik v covid-19 vaccine is 92% effective, 2020. URL: https://www.reuters.com/article/health-coronavirus-russia-vaccine/russia-says-its-sputnik-v-covid-19-vaccine-is-92-effective-idUSKBN27R0ZA, prees release, November 11, 2020.
[55] E. Cohen, Moderna's coronavirus vaccine is 94.5% effective, according to company data, 2020. URL: https://edition.cnn.com/2020/11/16/health/moderna-vaccine-results-coronavirus/index.html, prees release updated November 16, 2020.
[56] A. Chatzilena, E. van Leeuwen, O. Ratmann, M. Baguelin, N. Demiris, Contemporary statistical inference for infectious disease models using stan, Epidemics 29 (2019) 10036(1–16). doi:10.1016/j.epidem.2019.100367.
[57] Comisión Nacional de Vivienda, Proyecciones de población, Accesed November 2020. URL: https://sniiv.conavi.gob.mx/demanda/poblacion_proyecciones.aspx.

A. Parameter estimation

Mathematical models for COVID-19 have shown that the parameters' values are not necessarily the same in each country. We use COVID-19 data from Mexico City plus Mexico state to follow the epidemic curve's initial growth in this work. Consequently, we estimate some parameter values of system in Equation (1) [37]. To obtain the baseline parameter values, we consider two-stages: i) before and ii) after mitigation measures were implemented. For both stages, we use model in Equation (1) with no vaccination dynamics ($\lambda_V = 0$ and $V(0) = 0$), and STAN R-package. This package is used for statistical inference by the Bayesian approach. For the code implementation of our system, we follow ideas of [56], and it is made freely available at [46]. For this section, our estimations are focused on three parameters: β_A, β_S and p. Other parameter values are given in Table A.8.

Parameter	Value	References
δ_E^{-1}	5.1 days	[32]
α_S^{-1}	5.97 days	[15]
α_A^{-1}	10.81 days	[15]
δ_R^{-1}	365 days	
μ^{-1}	70 years	

Table A.8: Fixed parameters values of system in Equation (1).

For the first stage, the following system is considered:

$$\begin{aligned}
S'(t) &= \mu\bar{N} - \frac{\hat{\beta}_S I_S + \hat{\beta}_A I_A}{\bar{N}} S - \mu S + \delta_R R \\
E'(t) &= \frac{\hat{\beta}_S I_S + \hat{\beta}_A I_A}{\bar{N}} S - (\mu + \delta_E) E \\
I_S'(t) &= p\delta_E E - (\mu + \alpha_S) I_S \\
I_A'(t) &= (1-p)\delta_E E - (\mu + \alpha_A) I_A \\
R'(t) &= (1-\theta)\alpha_S I_S + \alpha_A I_A - (\mu + \delta_R) R \\
D'(t) &= \theta\alpha_S I_S
\end{aligned} \tag{A.1}$$

where $\bar{N}(t) = S(t) + E(t) + I_S(t) + I_A(t) + R(t)$ and $N = \bar{N} + D$. Here, we consider COVID-19 data from the first day of symptoms onset reported (February 19) until March 23, 2020. We also assume that $\theta = 0$ because the first reported death was on March 18, and there were three reported deaths until March 23. The initial values of recovered and dead people are set to zero. Symptomatic class initial value was fixed in one individual, while $E(0)$ and $I_A(0)$ were estimated. Thus, $S(0) = N - (E(0) + I_A(0) + 1)$, where $N = 26446435$ [57]. For the STAN implementation, we employ a negative-binomial model as the likelihood function with the mean parameter given by incidence solution per day. In addition to the above, we assign prior probability distributions to each parameter and the exposed and asymptomatic classes' initial conditions. Thus, we propose that $\hat{\beta}_A$ and $\hat{\beta}_S$ follow a normal distribution with parameters $\mu = 1$ and $\sigma^2 = 0.13$. Then, p follows a uniform distribution in $(0, 0.25)$, and $E(0)$ and $I_A(0)$ also follow a uniform distribution in $(2, 20)$ and $(2, 10)$, respectively. When employing our STAN implementation, we run 5 chains with 100,500 iterations each, discard the first 500, and use 10,000 samples to generate estimates of parameters $\hat{\beta}_A$, $\hat{\beta}_S$ and p. Table A.9 shows the confidence interval for each parameter and median posterior estimated.

Parameter	95% Confidence Interval	Quantile 50
$\hat{\beta}_S$	$[0.672, 1.1886]$	0.9322
$\hat{\beta}_A$	$[0.501, 0.7851]$	0.6435
p	$[0.061, 0.2206]$	0.1227
R_0	$[4.159, 5.1991]$	4.6082

Table A.9: Confidence interval and median posterior estimated for some parameters of system in Equation (A.1) and basic reproductive number (R_0).

For the second stage, we took a complete month starting the day when mitigation measures were implemented, that is, from March 23 to April 23, 2020. Now, we consider parameter ξ to model the implementation of non-pharmaceutical measures. Thus, system in Equation (A.1) becomes:

$$\begin{aligned}
S'(t) &= \mu\bar{N} - \frac{\xi\hat{\beta}_S I_S + \xi\hat{\beta}_A I_A}{\bar{N}} S - \mu S + \delta_R R \\
E'(t) &= \frac{\xi\hat{\beta}_S I_S + \xi\hat{\beta}_A I_A}{\bar{N}} S - (\mu + \delta_E) E \\
I_S'(t) &= p\delta_E E - (\mu + \alpha_S) I_S \\
I_A'(t) &= (1-p)\delta_E E - (\mu + \alpha_A) I_A \\
R'(t) &= (1-\theta)\alpha_S I_S + \alpha_A I_A - (\mu + \delta_R) R \\
D'(t) &= \theta\alpha_S I_S
\end{aligned} \tag{A.2}$$

where $\bar{N}(t) = S(t) + E(t) + I_S(t) + I_A(t) + R(t)$ and $N = \bar{N} + D$. At this stage, we consider that $\theta = 0.11$. Here, our objective is to estimate the value of parameter ξ. To do this, we use the median posterior of all the estimated parameters from the first stage (see Table A.9). Other parameter values are given in Table A.8. Almost all initial conditions were obtained when solving system in Equation (A.1) with the 10,000 samples (obtained in first stage), after which each solution at the final time (March 23) is saved. We use the median of the saved values. Thus, for system in Equation (A.2), $E(0) = 6587.585$, $I_S(0) = 553.7035$, $I_A(0) = 3149.924$, and $R(0) = 3001.547$. For the initial value of variable D, we consider reported COVID-19 data, then $D(0) = 3$. Therefore $S(0) = N - (E(0) + I_S(0) + I_A(0) + R(0) + D(0))$, with $N = 26446435$ [57]. Similar to the first stage, we consider a negative-binomial model as the likelihood function with the mean parameter given by incidence solution per day, while that we postulate a uniform distribution in $(0.25, 0.75)$ as a prior probability distribution for the parameter ξ. For the second stage, we run 5 chains with 100,500 iterations each, discard the first 500, and use 10,000 samples to generate estimates of parameters ξ. Table A.10 shows the confidence interval and median posterior estimated for parameter ξ.

Parameter	95% Confidence Interval	Quantile 50
ξ	$[0.3696, 0.4099]$	0.3889
R_0	$[1.702, 1.887]$	1.791

Table A.10: Confidence interval and median posterior estimated for parameter ξ of system in Equation (A.2) and basic reproductive number (R_0).

Finally, it is important to mention that our results were implemented considering that the effective transmission contact rates ($\beta_\bullet$) were equal to $\xi\hat{\beta}_\bullet$. This last means that our scenarios consider the first reduction in the effective transmission contact rates by NIPs. Using values in Tables A.9 and A.10, we build confidence intervals for $\xi\hat{\beta}_\bullet$. These results are shown in Table A.11.

Parameter	95% Confidence Interval
$\beta_S = \xi\hat{\beta}_S$	$[0.2483712, 0.48720714]$
$\beta_A = \xi\hat{\beta}_A$	$[0.1851696, 0.32181249]$

Table A.11: Confidence interval for parameters $\beta_\bullet$.

B. Positivity and Invariance of the Interest Region

Lemma 1. *The set* $\Omega = \{(S, E, I_S, I_A, R, D, V) \in \mathbb{R}^7_+ : S + E + I_S + I_A + R + D + V = N\}$ *is a positively invariant set for the system in Equation (1).*

Proof. Let $\Omega = \{(S, E, I_S, I_A, R, D, V) \in \mathbb{R}^7_+ : S + E + I_S + I_A + R + D + V = N\}$. First, note that for this model we have a closed population, which allows the solutions to be bounded superiorly by the total population.

On the other hand, to show the positivity of the solutions with initial conditions

$$(S(0), E(0), I_S(0), I_A(0), R(0), D(0), V(0)) \in \mathbb{R}^7_+,$$

we look at the direction of the vector field on the hypercube faces in the direction of each variable in the system. For example, consider a point on the hypercube face where the variable $S = 0$ and look at the behavior of the vector field in the direction of the same variable S, to see if the solutions cross the face of the hypercube where we are taking the initial condition. So, notice that if $S = 0$, $S'(t) > 0$, so the solution points into the hypercube. Similarly, consider an initial condition of the form $(S, 0, I_S, I_A, R, D, V)$ and note that $E'(t) > 0$ for all $t > 0$, which implies that the solutions of the system with initial conditions of the form $(S, 0, I_S, I_A, R, D, V)$ point towards the interior of the hypercube. Similarly, positivity can be tested for the rest of the variables. With this information, we have the following result. □

Now, continuing with the analysis of our model, it is easy to prove that the disease-free equilibrium is given by the point at $X_0 \in \Omega$ of the form

$$X_0 = \left(\frac{(\mu + \delta_V)\bar{N}}{\mu + \delta_V + \lambda_V}, 0, 0, 0, 0, \frac{\lambda_V \bar{N}}{\mu + \delta_V + \lambda_V}\right).$$

On the other hand, following ideas of [30], the next generation matrix for this model, evaluated in the disease equilibrium point, is given by

$$\mathbf{K} = \begin{bmatrix} \frac{\delta_E}{(\mu+\delta_E)}\left(\frac{p\beta_S}{\mu+\alpha_S+\mu_S+\lambda_T}\right)(S^*+\epsilon V^*) & \frac{\beta_S(S^*+\epsilon V^*)}{(\mu+\alpha_S+\mu_S+\lambda_T)\bar{N}} & \frac{\beta_A(S^*+\epsilon V^*)}{(\mu+\alpha_A+\mu_A)\bar{N}} \\ 0 & 0 & 0 \\ 0 & 0 & 0 \end{bmatrix} \tag{B.1}$$

where $S^* = \frac{(\mu+\delta_V)\bar{N}}{\mu+\delta_V+\lambda_V}$ and $V^* = \frac{\lambda\bar{N}}{\mu+\delta_V+\lambda_V}$. Then, the spectral radius of $\mathbf{K}$ is

$$R_V = R_S + R_A$$

with

$$R_S = \frac{p\beta_S\delta_E(\mu+\delta_V+(1-\epsilon)\lambda_V)}{(\mu+\delta_E)(\mu+\delta_V+\lambda_V)(\mu+\alpha_S)}$$
$$R_A = \frac{(1-p)\beta_A\delta_E(\mu+\delta_V+(1-\epsilon)\lambda_V)}{(\mu+\delta_E)(\mu+\delta_V+\lambda_V)(\mu+\alpha_A)}.$$